

**MASSACHUSETTS
INSTITUTE OF
TECHNOLOGY**



**SCHOOL OF
CHEMICAL
ENGINEERING
PRACTICE**

OAK RIDGE NATIONAL LABORATORY LIBRARIES



3 4456 0536840 1

S. M. SENKAN
DIRECTOR

J. P. McALEESE
ASSISTANT DIRECTOR

— SUMMARY OF PROJECTS —

SEPTEMBER 1977 - JUNE 1978

OAK RIDGE NATIONAL LABORATORY
OPERATED BY UNION CARBIDE CORPORATION • FOR THE DEPARTMENT OF ENERGY

Contents

	<u>Page</u>
1. Introduction	1
2. Summary of the Projects	5
A) Chemical Technology Division	5
1) Lime-Slurry Carbonation Reactors in Nuclear Fuel Reprocessing Plants	5
2) Cryogenic Vacuum Pumping in Fusion Reactors	7
3) Three-Phase Flow in Packed Beds	10
4) Mass Transfer in Three Phase Fluidized Beds	12
5) Recirculating Fluidized Beds	14
B) Chemistry Division	17
1) Surface Characteristics of Catalyst Supports	17
2) Physico-Chemical Characterization of Coal Surface	20
3) Dispersion of Miscible Fluids in Porous Media	26
4) Recovery of Uranium from Phosphate Rocks	29
C) Biology Division	31
Volume Restricted Freezing of Living Cells and Tissues	31
D) Energy Division	34
Energy and Cost Analysis of Room Air Conditioners	34
E) Engineering Technology Division	36
1) Radiation Cooling in LMFBR Cores	36
2) Supercooling of Water in ACES Heat Exchangers	39
F) Nuclear Medicine Technology	42
Design of a ^{18}F Production System for ORNL Cyclotron Facility	42

1. INTRODUCTION

The Massachusetts Institute of Technology School of Chemical Engineering Practice has been operating at Oak Ridge for over twenty six years. The school is designed to accelerate the development of highly competent masters-level engineers by providing them an intensive, guided program in which they develop:

- a) an ability to apply engineering principles to the solution of technical, industrial and research problems,
- b) a proficiency in effective oral and written communication skills,
- and c) a proficiency in human relations.

Practice School operation is as follows: student groups of two to four are assigned one-month projects suggested by the various departments of ORNL. The most important criteria in project selection is that it must be of educational value to the students and that the solution should require in-depth application of a broad variety of chemical engineering skills, original thought, initiative, and sound judgment. The plant personnel who suggest the particular problem are asked to serve as consultants. Once the problem is assigned the students, Practice School staff, consultants, and ORNL staff and personnel are considered a cooperative team whose job it is to solve the problem.

During the academic year 1977-78, a total of 35 students were involved in over 20 one-month projects, several of which were followups. Of these projects, five will be presented in outside professional symposiums and technical meetings.

Table 1 shows the distribution of MIT Practice School projects within ORNL. Approximately one third of the problem work was conducted in the Chemical Technology Division. Contributions included the analysis of a stirred tank carbonation reactor for the removal of radioactive carbon dioxide from the off-gases of nuclear reactor fuel reprocessing plants. Work in the controlled thermonuclear fusion reactor research involved the mathematical modeling of the helium-cooled cryosorption pumping process. Practice school contributions to coal research included the operation and mathematical modeling of a recirculating fluidized-bed reactor in which hydrodynamic parameters were studied. Mass transfer characteristics of

Table 1. Distribution of MIT Practice School Projects Within ORNL

ORNL Division	Consultants	Project	Date and ORNL/MIT-Report Number	Students
Chemical Technology	G.L. Haag D.W. Holladay A.D. Ryon	Lime-Slurry Carbonation Reactors in Nuclear Fuel Reprocessing Plants	9/6/77 - 256	J.P. McAleese, B.A. Belt, J.R. Datesh, M.C. Shaeffer
Chemical Technology	P.W. Fisher S.D. Clinton J.S. Watson J.B. Talbot	Cryogenic Vacuum Pumping in Fusion Reactors	4/28/78 - 275	J.R. Perini, Y.Y. Roberts, B.W. Wu
Chemical Technology	H.D. Cochran, Jr. E.L. Youngblood P.R. Westmoreland	Recirculating Fluidized Beds (Coal Pyrolysis)	3/3/78 - 269	M.Z. Khan, S.A. Berger, F.S. Gillet d'Auriac
Chemical Technology	J.M. Begovich S.D. Clinton J.S. Watson	Mass Transfer in Three Phase Fluidized Beds	4/4/78 - 272	B.W. Wu, Y.L. Cheng, J.R. Perini, J.L. Roux-Buisson
Chemical Technology	J.M. Begovich H.D. Cochran, Jr. G.E. Oswald	Three-Phase Flow in Packed Beds (Synthoil Process)	9/6/77 - 257	F. Barreto, S.J. Anderson, B.R. Goldstein, S.S. Moor
Biology	G.P. Hirsch	Freezing of Living Cells and Tissues	11/1/77 - 260 11/29/77 - 265	M.S. Giroux, G.M. Rinaldi, L.W. Bonnell S.D. Engstrom, Y.J. Chu, W.F. Sung
Chemistry	E.L. Fuller, Jr.	Surface Characteristics of Catalyst Supports	11/1/77 - 261	M.J. Abadi, W.F. Sung, C.T. Geary
Chemistry	E.L. Fuller, Jr.	Physico-Chemical Characterization of Coal	11/29/77 - 264 2/6/78 - 266 3/3/78 - 270 4/4/78 - 273	D.G. Sundberg, M.J. Abadi, M.S. Giroux M.M. Alger, O.K. Chow, M.Z. Khan L.A. Field, A.J. Papadopoulos, R.D. Wang R.N. Caron, K.J. Fallon, J.F. Orrik
Chemistry	S.Y. Shiao K.A. Kraus J.S. Johnson, Jr.	Dispersion in Miscible Fluids in Porous Media	9/29/77 - 259 4/28/78 - 276	S.S. Moor, S.J. Anderson, B.A. Belt, J.P. McAleese Y.L. Cheng, B. Budiman, M. Machbitz
Chemistry	W.D. Arnold F.J. Hurst O.L. Keller	Recovery of Uranium from Phosphate Rocks	2/6/78 - 267	R.D. Wang, L.A. Field, F.S. Gillet d'Auriac
Energy	E. Hirst D. O'Neal	Cost/Efficiency Analysis of Room Air Conditioners	2/6/78 - 268	A.J. Papadopoulos, S.A. Berger
Nuclear Medicine Technology	T.A. Butler J.K. Poggenburg B.W. Wieland	Design of a ^{18}F Production System for ORNL Cyclotron Facility	9/29/77 - 250 11/1/77 - 262	M.C. Shaeffer, F. Barreto, J.R. Datesh, B.R. Goldstein Y.J. Chu, S.D. Engstrom, D.G. Sundberg
Engineering Technology	E.C. Hise J.C. Moyers A.D. Solomon V. Baxter	Supercooling of Water in ACES Heat Exchangers	11/29/77 - 263	G.M. Rinaldi, L.W. Bonnell, C.T. Geary
Engineering Technology	J.T. Han M. Fontana	Radiation Cooling in LMFBR Cores	4/4/78 - 274	M. Machbitz, B. Budiman, Y.Y. Roberts

three-phase cocurrent fluidized beds were also investigated in relation to catalytic coal liquefaction processes. Hydrodynamic characteristics of three-phase flow in packed beds were investigated by simulating the operating conditions of the Synthoil coal liquefaction process.

Work in the Biology Division involved the testing of a new concept in cryogenic preservation. Aqueous solutions of living cells and organisms were frozen in stainless steel vessels at constant volume. The effects of cooling and warming rates and bath temperatures were examined in an attempt to maximize survival rates.

Practice School projects in the Chemistry Division involved the physico-chemical characterization of the surfaces of catalyst supports and a variety of coals. In relation to tertiary oil recovery processes, work was conducted on the dispersion phenomenon in miscible displacement in porous media. Another study investigated the economics of the recovery of uranium from phosphate rocks.

The Practice School contribution to the Energy Division was the energy/cost analysis of room air conditioners. As a result, a production possibilities curve was generated to be used in the ORNL energy model which simulates the energy use in the U.S. residential sector from 1970 to 2000.

Work in the Engineering Technology Division involved the examination of radiation cooling in voided liquid metal fast breeder reactor cores. The results provided a quantitative basis in making accurate safety and accident analyses in breeder reactor technology. Also, the supercooling phenomenon in Annual Cycle Energy System heat exchangers was investigated in an attempt to prolong the duration of this supercooling to increase heat transfer efficiency.

In a series of projects sponsored by the Nuclear Medicine Technology group, a ^{18}F production system was designed to be used at ORNL 86-inch cyclotron facility. This work was conducted in close association with the Medical Division of Oak Ridge Associated Universities.

In summary, the academic year 1977-78 has been highly successful, interesting, and productive. We are looking forward to a similar challenging and exciting year in 1978-79.

S.M. Senkan

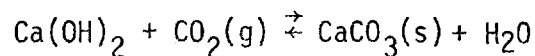
Oak Ridge
June 1978

2. SUMMARY OF THE PROJECTS

A. Chemical Technology Division

1) Lime-Slurry Carbonation Reactors in Nuclear Fuel Reprocessing Plants

Carbon-14 and krypton-85 are radioactive components of off-gas streams from nuclear reactor fuel reprocessing plants. Moderate levels of beta and gamma radiation from ^{85}Kr can damage living cells; however, ^{14}C presents a more serious problem as it can become incorporated into genetic material through the food cycle and cause mutations. The FASTER (Fluorocarbon Adsorption System for the Treatment of Effluents from Reprocessors) system removes carbon dioxide first by precipitating it as calcium carbonate (1). The reaction proceeds:



The ^{14}C removal system was simulated by a stirred tank containing a calcium hydroxide slurry through which gas containing CO_2 was bubbled, Fig. A1-1. Gas residence time distributions (RTDs) were determined as functions of gas flow rates and impeller speeds for inlet gas compositions of air with about 300 ppm CO_2 and for a mixture of 80% CO_2 and 20% O_2 . The carbonation reactor should ideally permit ^{85}Kr to pass through to a subsequent removal system. Mean residence times and dispersion coefficients were found to be inversely proportional to gas flow rates, slightly proportional to impeller speeds for air, and were poorly characterized for high carbon dioxide feeds. An empirical correlation was obtained:

$$X = a \frac{(\text{rpm})^n}{(\log \text{ mean } Q)^m}$$

where X is either the mean residence time or the dispersion coefficient of the gas, Q is the gas flow rate through the reactor, and rpm is the impeller speed. The letters a , m , and n are empirical constants which are different for air and CO_2 -rich gas (2).

The decontamination factors (DF) for krypton were also measured. DF is defined as the ratio of moles of ^{85}Kr entering to moles of ^{85}Kr leaving the gas flowing through the reactor. The DF values using 3% CO_2 ranged from 1.001 to 1.006. DF values corresponding to a CO_2 -rich feed gas were highly

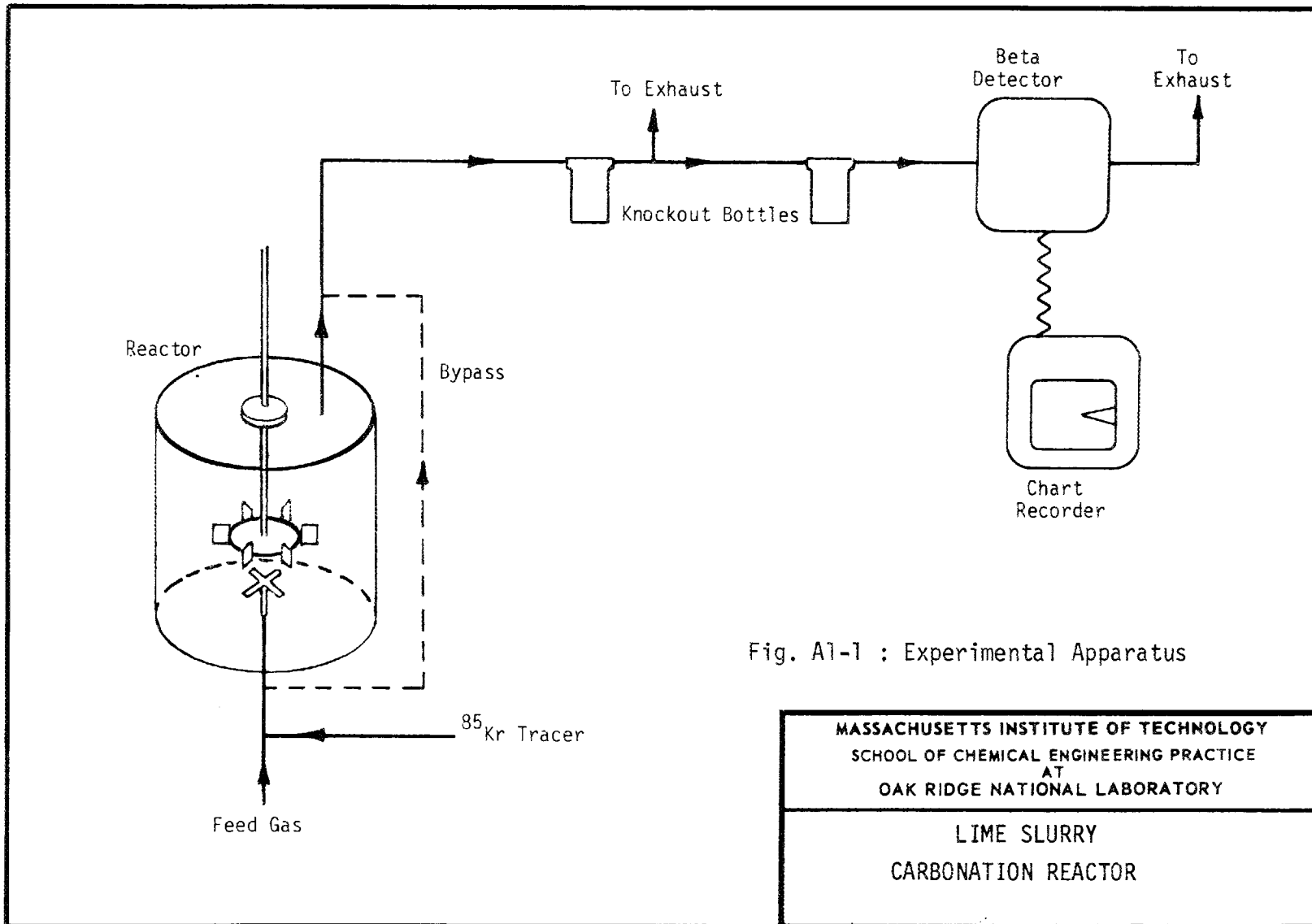


Fig. A1-1 : Experimental Apparatus

<p>MASSACHUSETTS INSTITUTE OF TECHNOLOGY SCHOOL OF CHEMICAL ENGINEERING PRACTICE AT OAK RIDGE NATIONAL LABORATORY</p>
<p>LIME SLURRY CARBONATION REACTOR</p>

irreproducible. However, preliminary results indicate that ^{85}Kr adsorbs on CaCO_3 in increasing quantities when CO_2 content of the feed gas is increased.

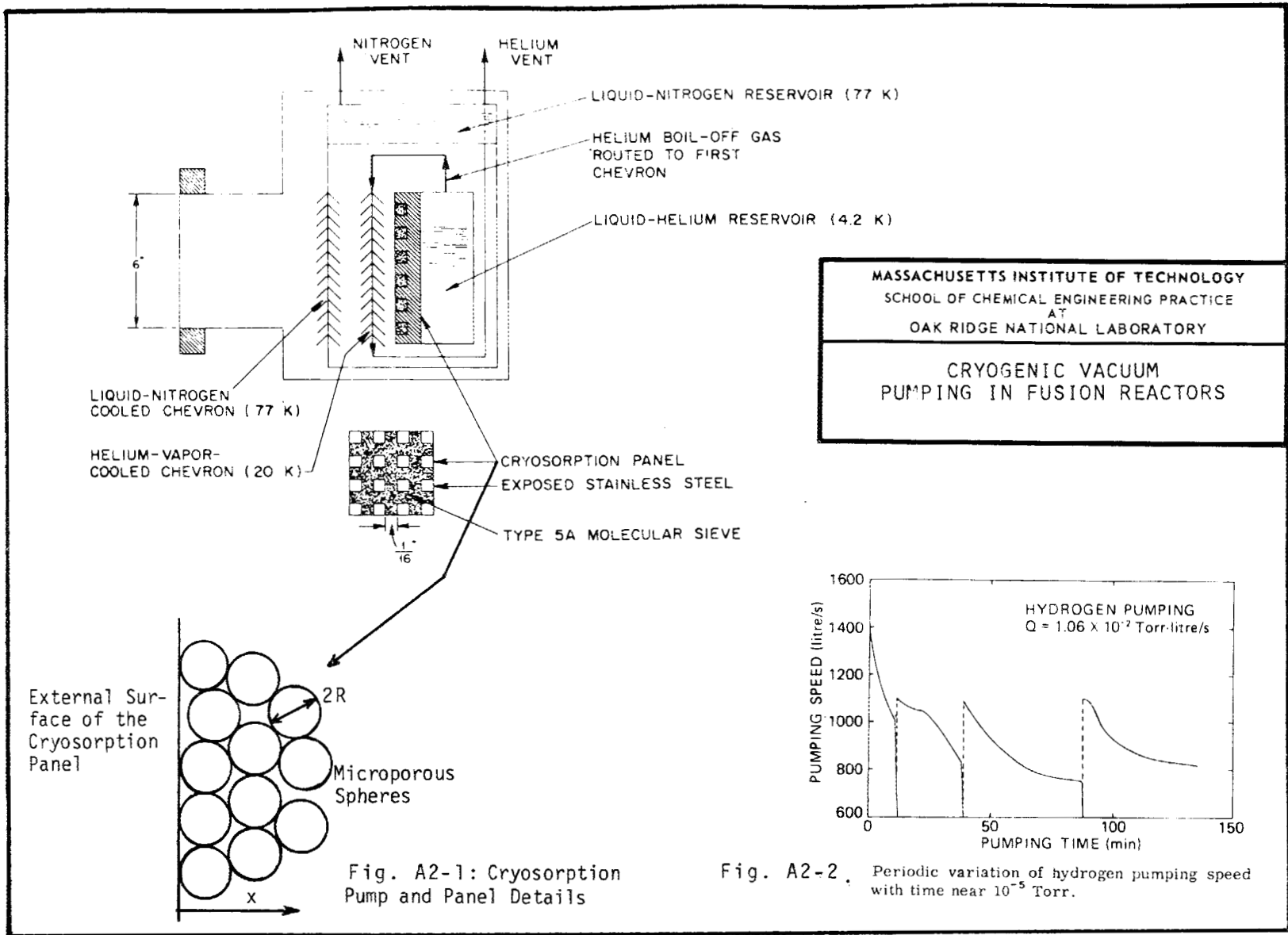
(1) Forsberg, C.W., "Theoretical Analysis and Preliminary Experiments on the Feasibility of Removing CO_2 Containing ^{14}C Selectively with a $\text{Ca}(\text{OH})_2$ Slurry from a ^{85}Kr -Contaminated HTGR Reprocessing Plant Off-Gas Stream," ORNL/TM-5825 (1977).

(2) McAleese, J.P., B.A. Belt, J.R. Datesh, and M.C. Shaeffer, "Analysis of Lime-Slurry Stirred Tank Carbonation Reactor," ORNL/MIT-256 (Sept. 1977).

2) Cryogenic Vacuum Pumping in Fusion Reactors

Vacuum requirements for Controlled Thermonuclear Reactors (CTRs) are different than those encountered in conventional high vacuum systems. The CTR vacuum pumps must operate in high magnetic and electrical fields; they should provide clean vacuum (i.e., no oil or mercury contamination) and be very reliable. Cryogenic vacuum pumps fulfill all these requirements. These pumps operate by accumulating gases from a vacuum system onto a cold surface either by plain condensation mechanism (cryocondensation) or by physical adsorption on porous materials such as molecular sieves (cryosorption) (see Fig. A2-1).

Preliminary experiments with deuterium (using liquid He at 4.2 K) showed that constant pumping speeds can be maintained for pressures up to 10^{-4} torr. Since the vapor pressure of deuterium is 3.6×10^{-11} torr at 4.2 K, the pumping mechanism is mainly cryocondensation. However, for H_2 and He (vapor pressures of 10^{-6} torr and 1 atm respectively at 4.2 K) pumping speed shows a peculiar cyclic behavior. For a period of time pumping speed decreases monotonically, usually to a value 1/2 to 1/10 of the initial speed, followed by a sharp recovery period. The whole process then repeats itself. Diffusion limitations of H_2 and He into the zeolite bed have been suggested to be the cause of this cyclic phenomenon (1). Accordingly, high H_2, He pumping speeds were attributed to accumulation in the surface cavities of the adsorbent such that when these cavities become filled, the pumping speed declines. The reduction in pumping speed then rapidly increases the back pressure and then temperature to 10^{-2} torr and



10-20 K respectively, resulting in an increase in diffusion rates into the adsorbent. The cycle then repeats itself (see Fig. A2-2).

Mass transfer into the zeolite cryosorption panel was investigated by modeling it as a bidisperse (macro/micro) porous structure. In the macropores Knudsen diffusion dominates which permits the transport of gases into the bed. The micropores within the zeolite beads are characterized by the activated diffusion process. The gas composition in the macropores was assumed to be in equilibrium with the external surface of the beads. Unsteady state material balance in macropores results in the following:

$$\frac{\partial C_A}{\partial t} = D_k \frac{\partial^2 C_A}{\partial x^2} - \frac{D_i}{R} \left. \frac{\partial C_i}{\partial r} \right|_{r=R}$$

similarly for the micropores,

$$\frac{\partial C_i}{\partial t} = D_i \frac{1}{r^2} \frac{\partial}{\partial r} \left(r^2 \frac{\partial C_i}{\partial r} \right)$$

where C_A , C_i , and D_k , D_i are the concentration and diffusion coefficients in the macropores and micropores, respectively. x is the position coordinate through the panel and r is the radial position within the microsphere. Usual symmetry and relevant boundary conditions were used (1). The equilibrium relationship between C_i and C_A is given by the isotherm relationships,

$$\begin{aligned} C_i(t, r=R, x) &= f[C_A(x, t)] \\ &= \frac{aC_A(x, t)}{1+bC_A(x, t)}, \text{ Langmuir isotherm} \end{aligned}$$

Two limiting cases were examined: (1) diffusion into the cryosorption panel is infinitely fast; hence, the rate of adsorption is limited by diffusion into the microporous crystallites, (2) diffusion into the microporous beads is infinitely fast; therefore the rate of adsorption is limited by diffusion into the panel. Various analytical solutions were obtained (2) following several simplifying assumptions.

(1) Fisher, P.W., and J.S. Watson, "Cryosorption Vacuum Pumping of Deuterium, Helium, and Hydrogen at 4.2 K for CTR Applications," Proc. 24th Conf. Remote Syst. Tech., 1976.

(2) Perini, J.R., Y.Y. Roberts, and B.W. Wu, "Cryogenic Vacuum Pumping," ORNL/MIT-275 (April 1978).

3) Three-Phase Flow in Packed Beds

The Synthoil process involves the reaction of coal-oil slurry contacted cocurrently with hydrogen gas. The reaction takes place at elevated temperatures and pressures in a fixed bed catalytic reactor (1). It has been found that significant reaction may occur even in the absence of any catalyst other than the mineral matter found in coal (2).

Microscale turbulence is desirable in all gas-solid-liquid reactions since it promotes phase contact (3, 4). Macroscale turbulence is undesirable as it causes dispersion (backmixing), hence reducing the yield. Therefore, conversion may be improved by minimizing dispersion and by maximizing micromixing.

Coal-water/glycerine slurries (35% coal) were used to simulate the Synthoil process feed streams. The slurry was treated as a quasi-one-phase system because of its homogeneity and because coal-liquid density differences were small. Slurry dispersion was examined utilizing the dispersed plug flow model (5).

It was shown that for an unpacked column in the laminar flow regime, increasing liquid viscosity increases axial dispersion (see Fig. A3-1), energy dissipation, and to a small extent the liquid saturation. However, in packed columns viscosity had no apparent effect on dispersion (Fig. A3-2). Alternatively, in packed columns, increasing gas flow rates had little effect on axial dispersion and liquid saturation, but it did increase energy dissipation.

Additionally, vessels with cylindrical packing exhibited marked differences from systems using spherical packing. Energy dissipation and liquid saturation were much greater in vessels packed with cylinders; this was attributed to the inherent close packings (small void volumes) encountered in cylinder packed columns.

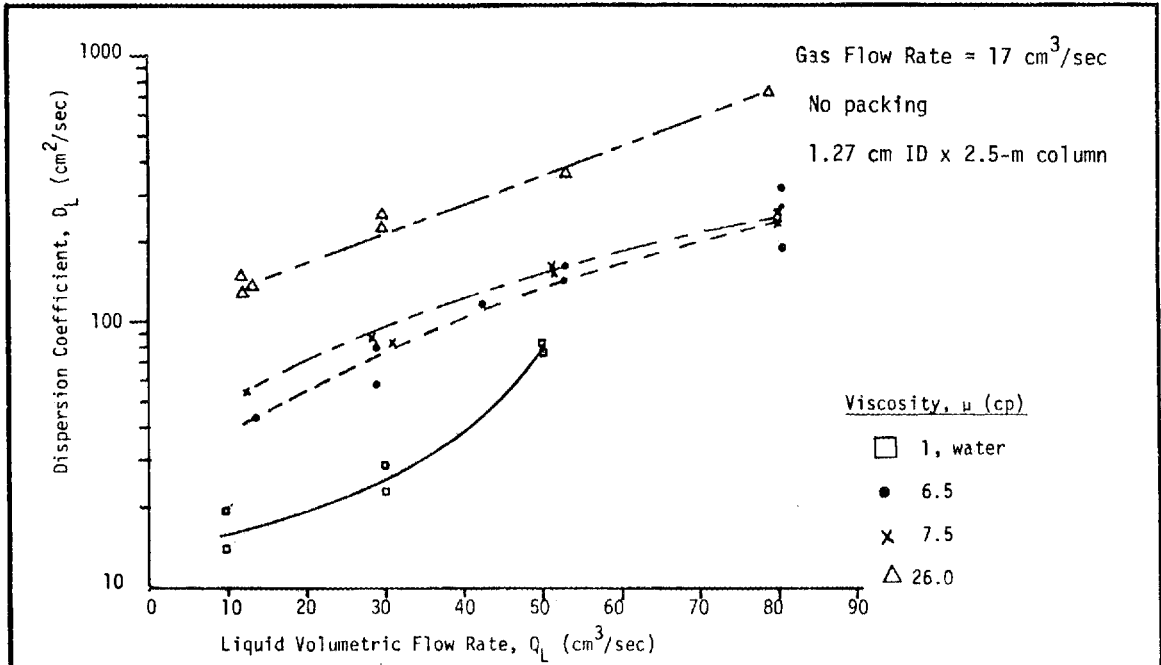


Fig. A3-1, DISPERSION COEFFICIENT VS SLURRY FLOW RATE AT DIFFERENT SLURRY VISCOSITIES

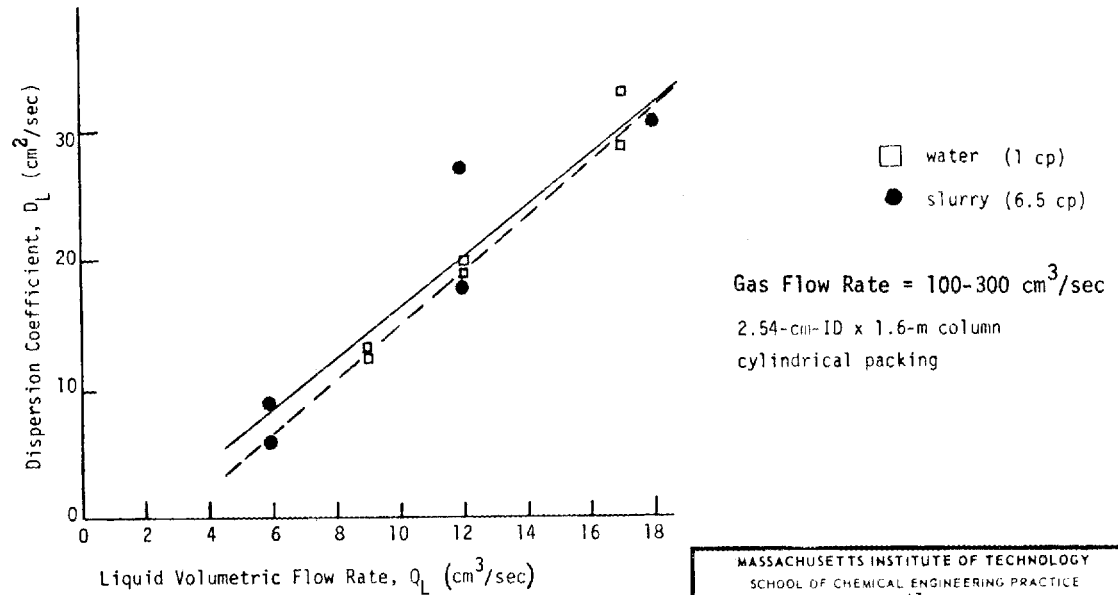


Fig. A3-2. DISPERSION COEFFICIENT VS LIQUID FLOW RATE

MASSACHUSETTS INSTITUTE OF TECHNOLOGY
SCHOOL OF CHEMICAL ENGINEERING PRACTICE
AT
OAK RIDGE NATIONAL LABORATORY

THREE-PHASE FLOW IN
PACKED BEDS

(1) Brenner, H., D.C. Prieve, and B. Fitch, "Synthoil Hydrodynamics, Final Report," Prepared for ERDA Under Contract E(36-2)-0056, Dept. Chem. Eng., Carnegie-Mellon Univ., Pittsburgh, Pa. (March 1977).

(2) Wender, I., "Internal Quarterly Technical Progress Report, July-September 1976," PERC/QTR-76/3.

(3) Hirose, T., M. Toda, and Y. Sato, "Liquid Phase Mass Transfer in Packed Bed Reactor with Cocurrent Gas-Liquid Downflow," J. Chem. Eng., Japan, 7(3), 187 (1974).

(4) Reiss, L.P., "Cocurrent Gas-Liquid Contacting in Packed Columns," I&EC Proc. Des. Dev., 6(4), 486 (1967).

(5) Barreto, F., S.J. Anderson, B.R. Goldstein, and S.S. Moor, "Three-Phase Flow Characteristics of Cylindrical Vessels," ORNL/MIT-257 (Sept. 1977).

4) Mass Transfer in Three-Phase Fluidized Beds

Three-phase fluidized beds, in which solid particles are fluidized by cocurrent upflow of liquids and gases, are finding increased use in chemical reaction engineering (1, 2). Successful operation of many industrially-important reactions, such as liquefaction of coal, slurry methanation of CO, etc., depends on the proper understanding of the hydrodynamics and the mass-transport phenomena in these vessels.

Mass transfer experiments were conducted with two cocurrent three-phase fluidized beds (see Fig. A4-1). The liquid phase (aqueous glycerol) was saturated with oxygen prior to desorption by the inert gas phase (N₂ or Ar) inside the fluidized beds. Axial oxygen concentration profiles of the liquid were measured with oxygen analyzers. These profiles were then matched to mathematical model predictions to calculate liquid dispersion coefficients and overall mass transfer coefficients (3). The mathematical model was developed by assuming steady state operation, gas phase in plug flow regime, liquid phase in dispersed plug flow mode which can be characterized by a constant axial dispersion coefficient (E_L), a constant overall mass transfer coefficient ($K_L a$), and uniform fluidization throughout the bed (1).

The overall mass transfer coefficients increased with both increasing particle diameter and superficial gas velocity (see Figs. A4-2 and A4-3). However, no relationship between liquid velocity and $K_L a$ was observed.

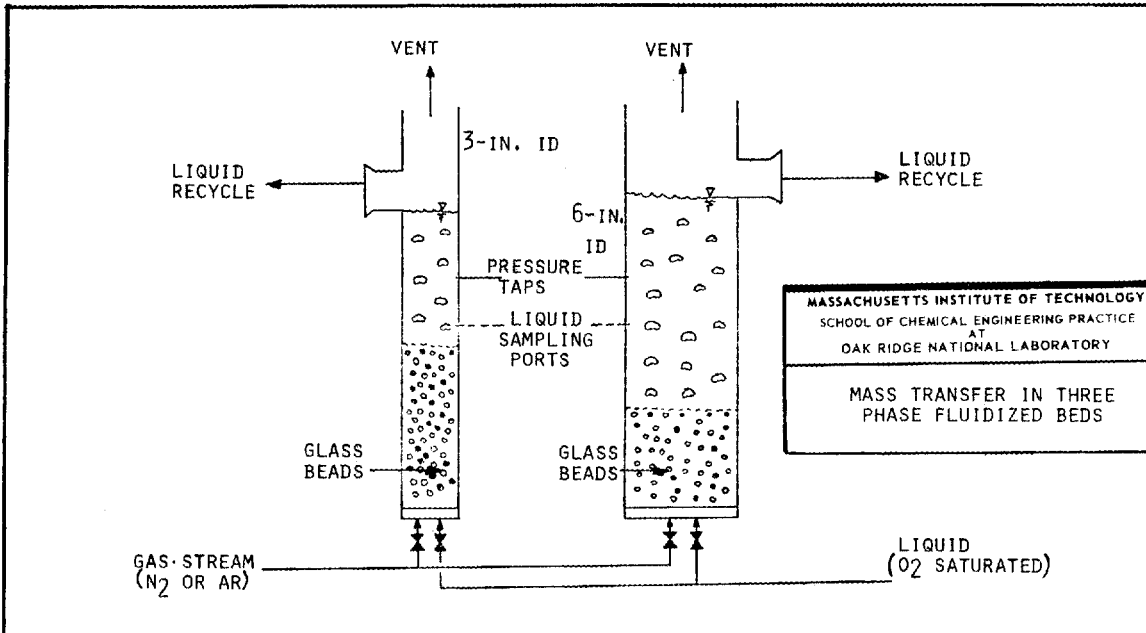


FIG. A4-1 THREE-PHASE FLUIDIZED BED SYSTEM

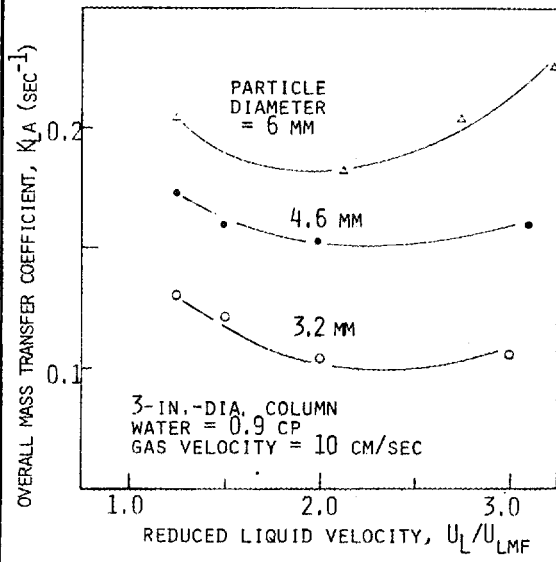


FIG. A4-2. EFFECT OF PARTICLE DIAMETER ON K_LA

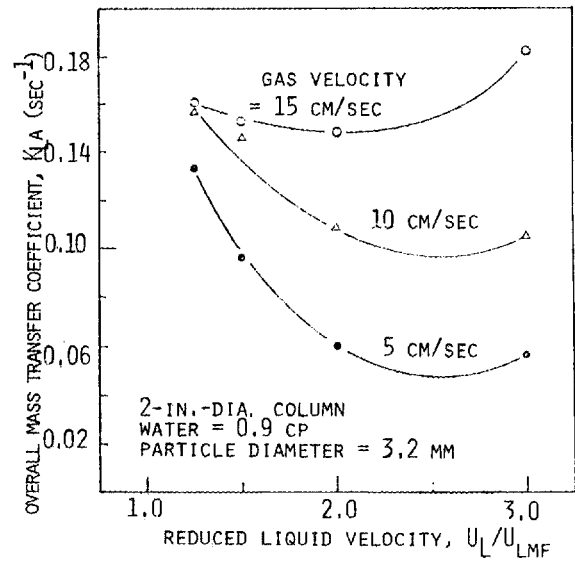


FIG. A4-3. EFFECT OF SUPERFICIAL GAS VELOCITY ON K_LA

$K_L a$ for the more viscous (2.4 cp) solution was lower than that for water (0.9 cp) at low liquid flow rates. However, the opposite situation was observed at high liquid flow rates. The liquid phase axial dispersion coefficient also increased on increasing the vessel diameter. Various recommendations were made for future work and equipment modifications.

(1) Ostergaard, K., "Gas-Liquid-Particle Operations," Adv. Chem. Eng., 7, 71 (1968).

(2) Ostergaard, K., "Holdup, Mass Transfer and Mixing in Three-Phase Fluidized Beds," Paper presented at AIChE 69th Meeting, Chicago, Nov. 28 - Dec. 2, 1976.

(3) Wu, B.W., Y.L. Cheng, J.R. Perini, and J.L. Roux-Buisson, "Mass Transfer Characteristics in Three-Phase Fluidized Beds," ORNL/MIT-272 (April 1978).

5) Recirculating Fluidized Beds

Many types of coal undergo plastic deformation above 200°C, which causes agglomeration, leading to frequent shutdowns of hydrocarbonization reactors. To avoid this, a recirculating fluidized bed with an axially-mounted draft tube has been developed (1). A mixture of hydrogen and finely ground coal is fed to the reactor through a jet, supplemented by a hydrogen stream from a second concentric, annular jet. The mixture enters the draft tube and mixes with hot, recirculating solid char from the mildly fluidized downcomer. The char minimizes contact between coal particles, preventing agglomeration, and rapidly heats the coal. Reaction occurs around 600°C and 20 atm. The gaseous products leave the draft tube, exit the reactor, and are condensed. The char enters the downcomer from which excess char is also withdrawn.

The hydrodynamics of a recirculating fluidized-bed hydrocarbonization reactor were studied in a 1-atm full-scale cold model. The clear plastic model was 4-in.-ID x 110-in.-tall with a 1-in.-OD axially-mounted draft tube (see Fig. A5-1). The bed consisted of char, as in the case of the high-pressure hydrocarbonization reactor, fluidized with air. Nitrogen was used in the draft tube so that bypass of gas from the plenum to the draft tube could be measured using an oxygen analyzer (2).

MASSACHUSETTS INSTITUTE OF TECHNOLOGY
 SCHOOL OF CHEMICAL ENGINEERING PRACTICE
 AT
 OAK RIDGE NATIONAL LABORATORY

RECIRCULATING FLUIDIZED BED

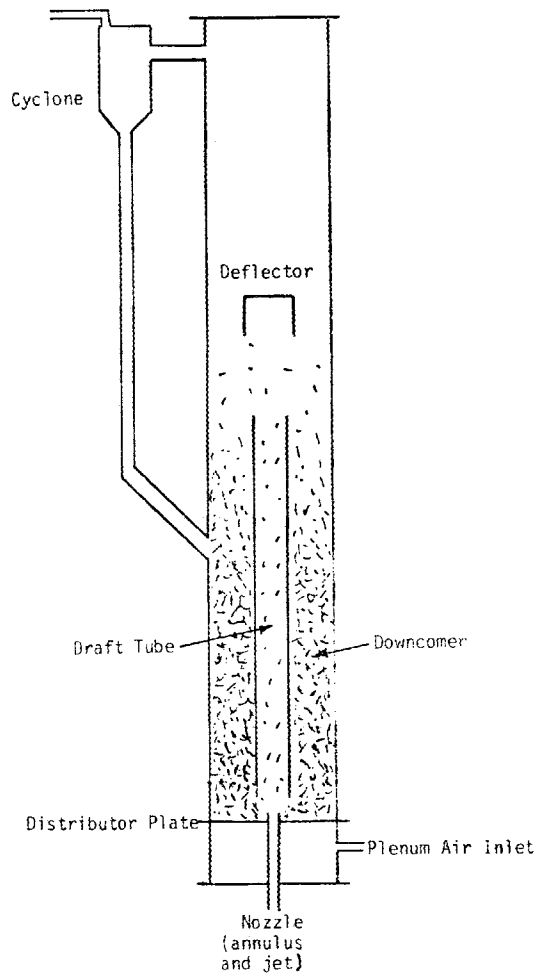


FIG. A5-1: SCHEMATIC DRAWING OF RECIRCULATING FLUIDIZED BED

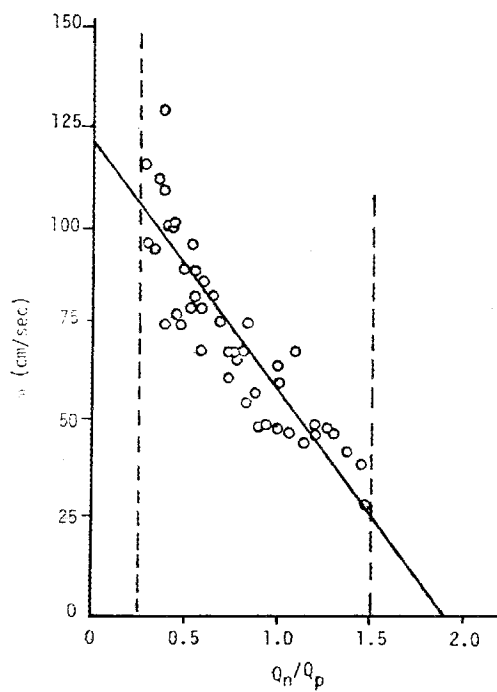


FIG. A5-2: RECIRCULATION RATE VS FLOW RATIO

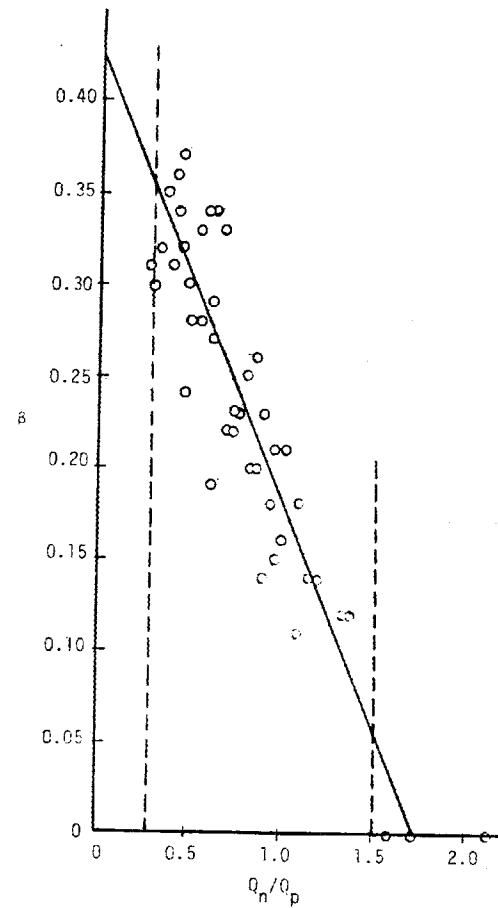


FIG. A5-3: BYPASS FRACTION OF Q_p VS FLOW RATIO

After determining the regions of stable operation, correlations were obtained for solids recirculation rate, fraction of plenum gas bypassing, and bottoms-region pressure drop as functions of the ratio of nozzle-to-plenum flow rates. Recirculation rate, W , was correlated by

$$W = 120.43 - 63.47 \frac{Q_n}{Q_p} \text{ gm/sec} \quad (\text{see Fig. A5-2})$$

The bypass fraction, β , was given by

$$\beta = 0.423 - 0.243 \frac{Q_n}{Q_p} \quad (\text{see Fig. A5-3})$$

The bottoms region pressure drop, as measured between the bottom of the downcomer and bottom of the draft tube, was given by

$$\Delta P_{\text{bot}} = 8000 - 6400 \frac{Q_n}{Q_p} \text{ dynes/cm}^2$$

The above correlations are good only for the stable operating region, which is bounded by Q_n/Q_p between 0.25 and 1.5. The pressure drop in the draft tube was found to be a sharply decreasing function of superficial velocity, indicating a fast-fluidized-bed behavior rather than a pneumatic transport line as previously considered (3).

Downcomer pressure drop vs superficial velocity also showed a similar behavior. This phenomenon was explained in relation to the downward sloping portion of the forward hysteresis loop in a fluidization diagram (ΔP vs velocity). Here, particles that were packed together began to unpack rapidly as gas velocity was increased and as fluidization began.

(1) Holmes, J.M., et al., "Hydrocarbonization Process Evaluation Report," ORNL-5212 and -5213 (1977).

(2) Khan, M.Z., S.A. Berger, and F.S. Gillet d'Auriac, "Hydrodynamics of Recirculating Fluidized Bed, Coal Hydrocarbonization Reactors," ORNL/MIT-269 (March 1978).

(3) Yang, W-C., and O.L. Keairns, "Comparison of Recirculating Fluidized Bed Performance in Two-Dimensional and Three-Dimensional Beds," in "Fluidization Technology," Vol. 2, D.L. Keairns, ed., p. 51, McGraw-Hill, New York, 1976.

B. Chemistry Division

1) Surface Characteristics of Catalyst Supports

Proper characterization of porous catalysts is important in chemical reaction engineering. It is essential to know surface areas, pore volume, catalyst dispersions, catalyst-support interactions, etc. to understand and formulate the processes involved in their use.

Cobalt oxide-molybdenum oxide catalysts, supported by silica-promoted alumina, are important in production of clean fuels from coal. Recently the possibility of an intimate relationship between catalytic activity of Co-Mo and the catalyst support was indicated (1). Therefore, studying the surface properties of silica-promoted alumina (6% SiO₂ on Al₂O₃), A6S, and comparing these results with previous data on Co-Mo- γ -Al₂O₃/SiO₂, CM3, was essential. Nitrogen adsorption/desorption experiments were performed to determine surface areas by monitoring the nature and rate of desorption, and by measuring the heats of immersion in water (2).

Surface areas obtained from nitrogen isotherms using the Brunauer-Emmett-Teller (BET) equation, constructed at increasing outgassing temperatures (OGT) of 25, 60, 100, 150, 200, 300, and 400°C, increased from 175 to 205 m²/gm (see Fig. B1-1). This increase was attributed to generation of additional surface area rather than creation of micropores as shown by t-plot diagrams (Fig. B1-2). Capillary condensation and hysteresis phenomena in mesopores seemed to be unaffected by OGT and occurred reproducibly in the P/P₀ range of 0.52 to 0.94 (see Fig. B1-3). When compared to the Co-Mo-SiO₂-Al₂O₃ catalyst, the support consistently had 5 to 10 m²/gm higher BET area for the OGT range investigated (see Fig. B1-1).

Mass spectra obtained at OGTs of 23-400°C indicated that water was the predominant species evolved (~95%), followed by increasing amounts of CO₂ (~5%). Plots of log signal intensities versus log time were linear, indicating that a well-defined mechanism of gas evolution was present. Correlation of the initial signal intensities and the slopes of these plots suggest that two mechanisms of desorption may be present: one below 200°C and one above 250°C.

Calorimetric measurements of the total heats of immersion of the samples in water at 25°C increased from 0.16 to 0.55 J/m² as the OGT increased,

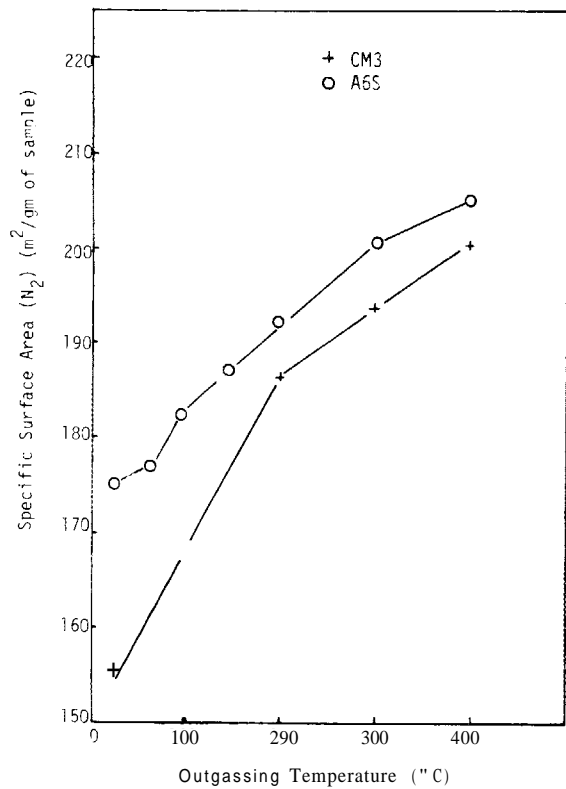


Fig. 81-1:
Comparison of Specific Surface
Area (BET) of CM3 and A6S at
Various Outgassing Temperatures (1)

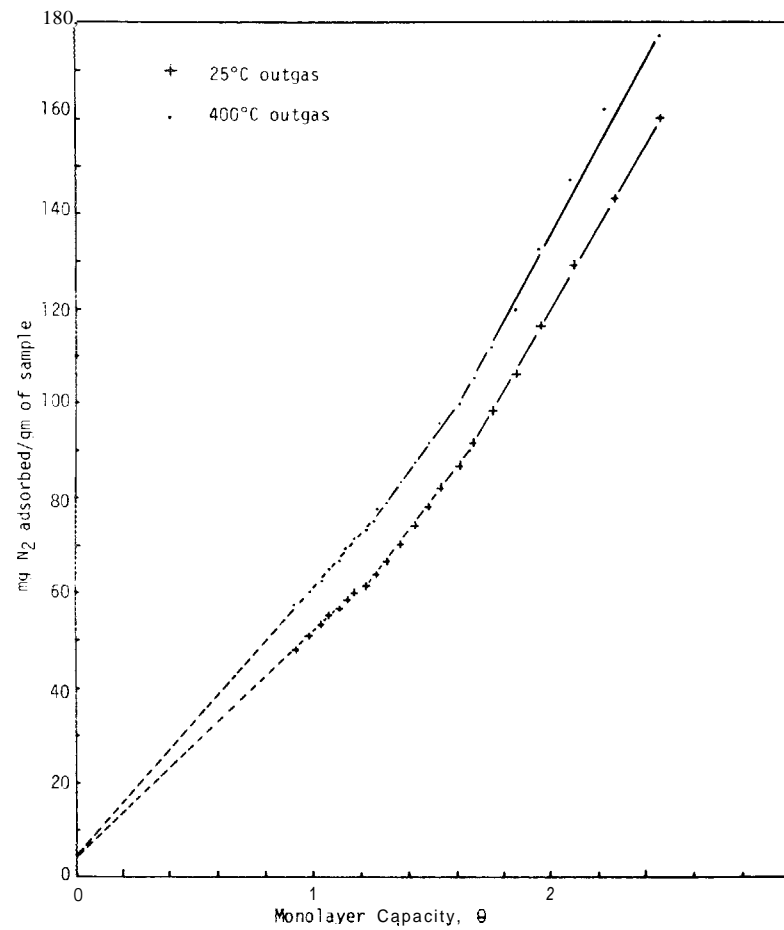


Fig. 81-2:
t-plots for
A6S Catalyst (1)

MASSACHUSETTS INSTITUTE OF TECHNOLOGY
SCHOOL OF CHEMICAL ENGINEERING PRACTICE
AT
OAK RIDGE NATIONAL LABORATORY

SURFACE CHARACTERISTICS
OF CATALYST SUPPORTS

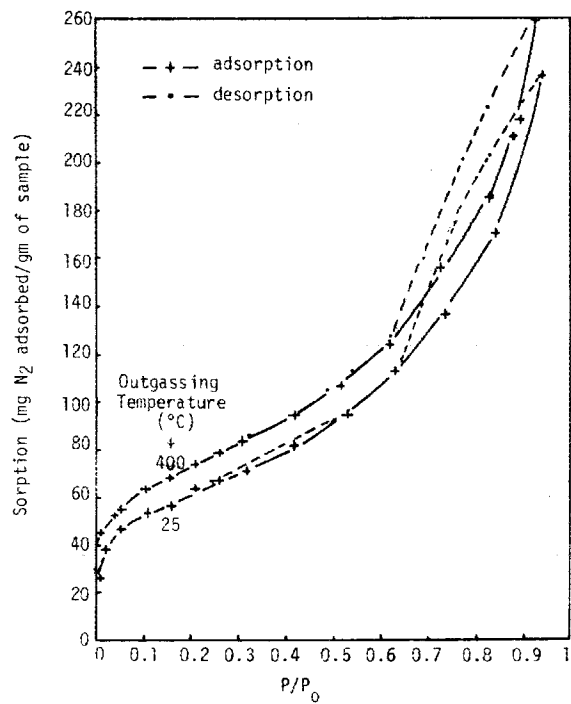


Fig. B1-3:
Nitrogen Sorption by A6S

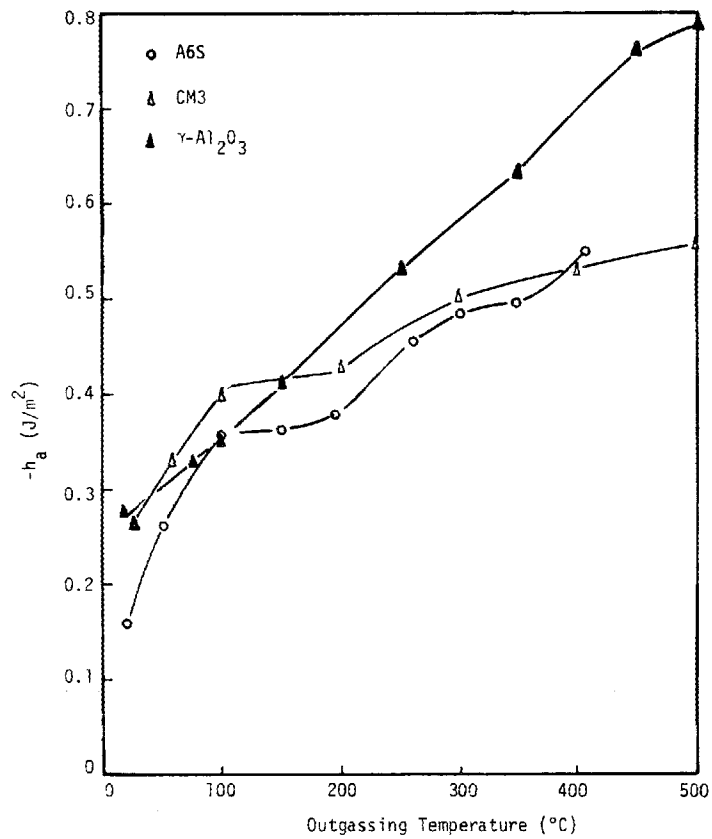


Fig. B1-4:
Total Heats of Water
Immersion of A6S, CM3,
and γ -Al₂O₃ at 25°C

MASSACHUSETTS INSTITUTE OF TECHNOLOGY
SCHOOL OF CHEMICAL ENGINEERING PRACTICE
AT
OAK RIDGE NATIONAL LABORATORY

SURFACE CHARACTERISTICS
OF CATALYST SUPPORTS

with a well-defined plateau between 100 to 200°C OGT at 0.35 J/m². A similar phenomenon was also observed at 350°C, which had not been observed previously for the Co-Mo catalyst (see Fig. B1-4). Slow heats of immersion showed a peak at 250°C OGT and 0.1335 J/m² with a half-life of 42 sec. Variation of the half-lives of the slow heats of immersion was apparently inversely proportional to the OGT for values above 150°C, with values as high as 252 sec at 150°C to 32 sec at 400°C.

(1) Fuller, E.L., and P.A. Agron, "Surface Properties and Reactions of Co-Mo Hydrotreating Catalyst: Preliminary Results," ORNL-5168 (1976).

(2) Abadi, J.J., C.T. Geary, and W.F. Sung, "Characterization of Catalysts and Catalyst Support Interactions," ORNL/MIT-261 (Nov. 1977).

2) Physico-Chemical Characterization of Coal Surface

Effective utilization of coal heavily depends on proper understanding of the surface properties of this solid fuel at the point of consumption (i.e., boilers, gasifiers, etc.). These surface properties may vary considerably as coal reacts with atmospheric vapors (O₂, CO₂, N₂, and H₂O) during its transportation from the mines and while it is being processed for use (grinding, drying, slurring, etc.).

It is generally accepted that a major portion of the carbon in coal is part of a network of polynuclear aromatic compounds (1). Coal also possesses a wide spectrum of pore structure (2, 3, 4) with pore sizes ranging from values less than 20 Å (micropores) to greater than 150 Å (mesopores) with surface areas ranging from 1-10 to 200-300 m²/gm (depending on methods used). Vapors must pass in or out of these pores during pyrolysis, chemical reaction, and sorption processes. Most of the moisture in coal also resides in these pores.

Abundant information exists regarding the nature of coal obtained by degradative processes such as oxidation and/or pyrolysis which have altered the original structure. Studies relating to the surface properties and reactivities of coal under non-destructive conditions are relatively rare. Several MIT Practice School teams have examined bituminous coals from Illinois (5, 6) and Pennsylvania (7), and Wyodak coal (8). Experimental work involved microgravimetric, mass spectroscopic, and calorimetric

techniques. BET surface areas, rates of adsorption and desorption of various gases, the nature of species desorbed, and heats of immersion in water were determined (see Table B2-1).

Table B2-1. Surface Properties of Coals Tested

Coal	Sorbates, Temperature (°C)	BET Area (m ² /gm)	Heats of Immersion ΔH_w (J/gm Sample)
Bruceton, Pa.	N ₂ -196	3.9	~ 12 - 14
	CO ₂ -78	144	
Illinois #6	N ₂ -196	2.9	~ 25
	CO ₂ -78	128	
	H ₂ O 23	68.2	
Wyodak	N ₂ -196	2.62	~ 120
	CO ₂ -78	200	
	H ₂ O 23	274	
	CO -183	2.1	
	N ₂ -183	1.6	

For all coals examined, CO₂ and H₂O adsorptions were considerably higher than that for N₂ (see Figs. B2-1 through B2-6). In addition, the nature of adsorption and the "hysteresis" phenomenon were entirely different in each case indicating the heterogeneous nature of the coal surface. Kinetics of adsorption of these gases were also different. CO₂ adsorption rates for Wyodak coal were successfully correlated by Fick's second law of diffusion:

$$\frac{\partial C}{\partial t} = D \frac{1}{r^2} \frac{\partial}{\partial r} (r^2 \frac{\partial C}{\partial r}) \quad (\text{see Fig. B2-7})$$

The diffusion coefficients were calculated to be on the order of 10⁻⁷ cm/sec and they were pressure insensitive with a weak, increasing dependency on temperature (8). On the other hand, H₂O sorption rates did not follow the rates predicted by Fick's law; however, they were successfully correlated by a second order process given by

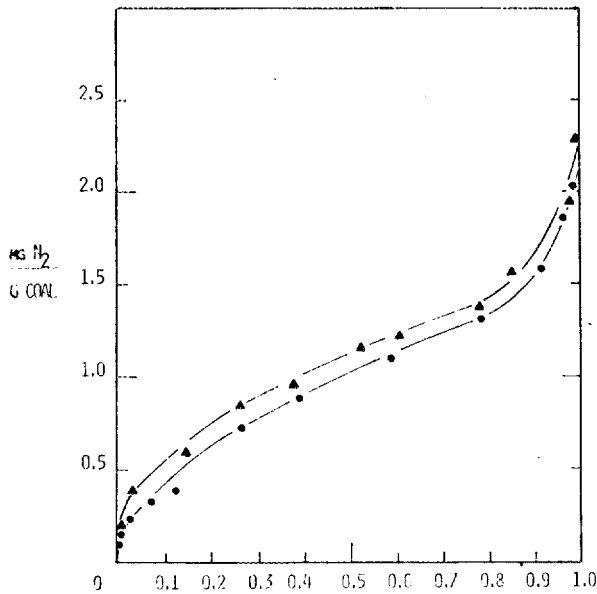


Fig. B2-1: N₂ Isotherm (-196°C) Wyodak Coal

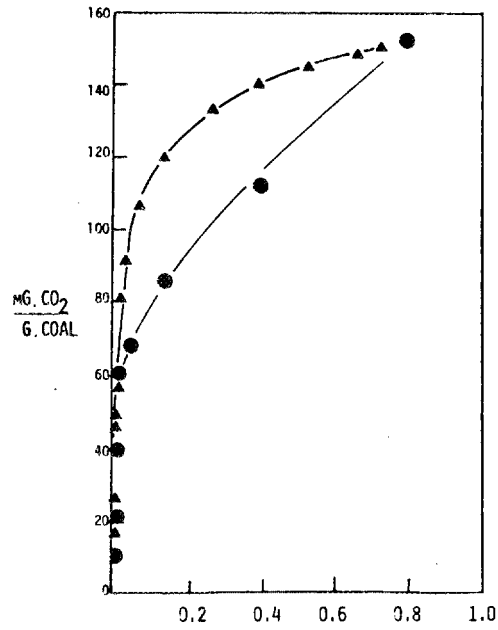


Fig. B2-2: CO₂ Isotherm (-78°C) Wyodak Coal

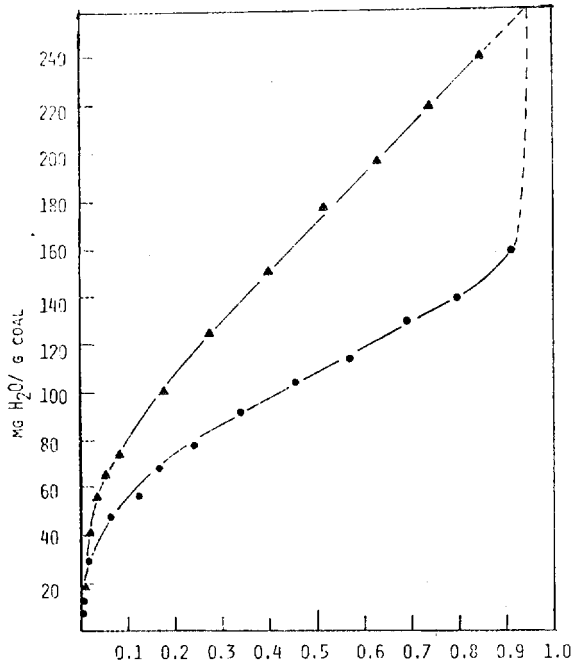


Fig. B2-3: H₂O Isotherm (20°C) Wyodak Coal

● ADSORPTION
▲ DESORPTION

MASSACHUSETTS INSTITUTE OF TECHNOLOGY
SCHOOL OF CHEMICAL ENGINEERING PRACTICE
AT
OAK RIDGE NATIONAL LABORATORY
PHYSICO-CHEMICAL CHARACTERIZATION
OF COAL

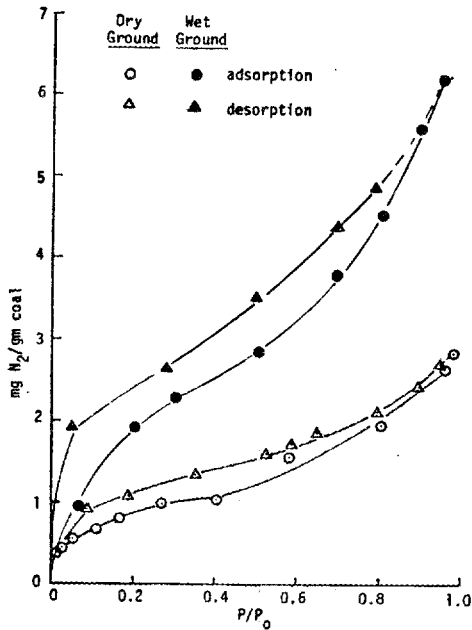


Fig. B2-4: N₂ Sorption Isotherms (-196°C), I-6 Coal

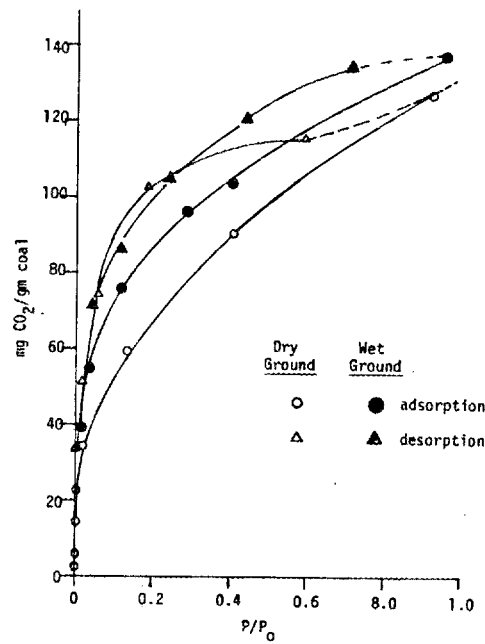


Fig. B2-5: CO₂ Sorption Isotherms (-78°C), I-6 Coal

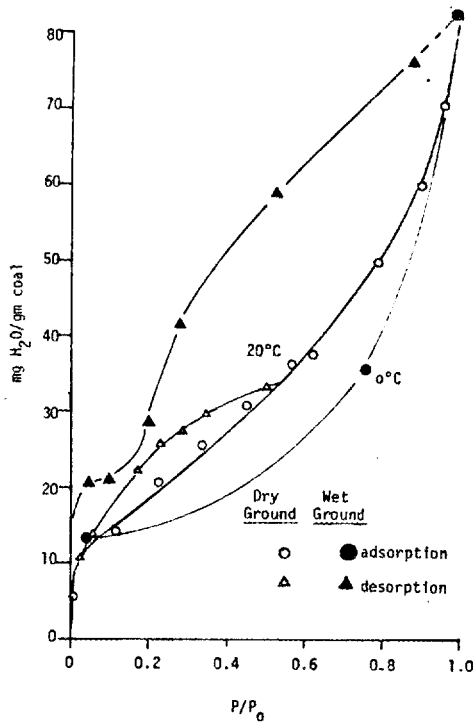
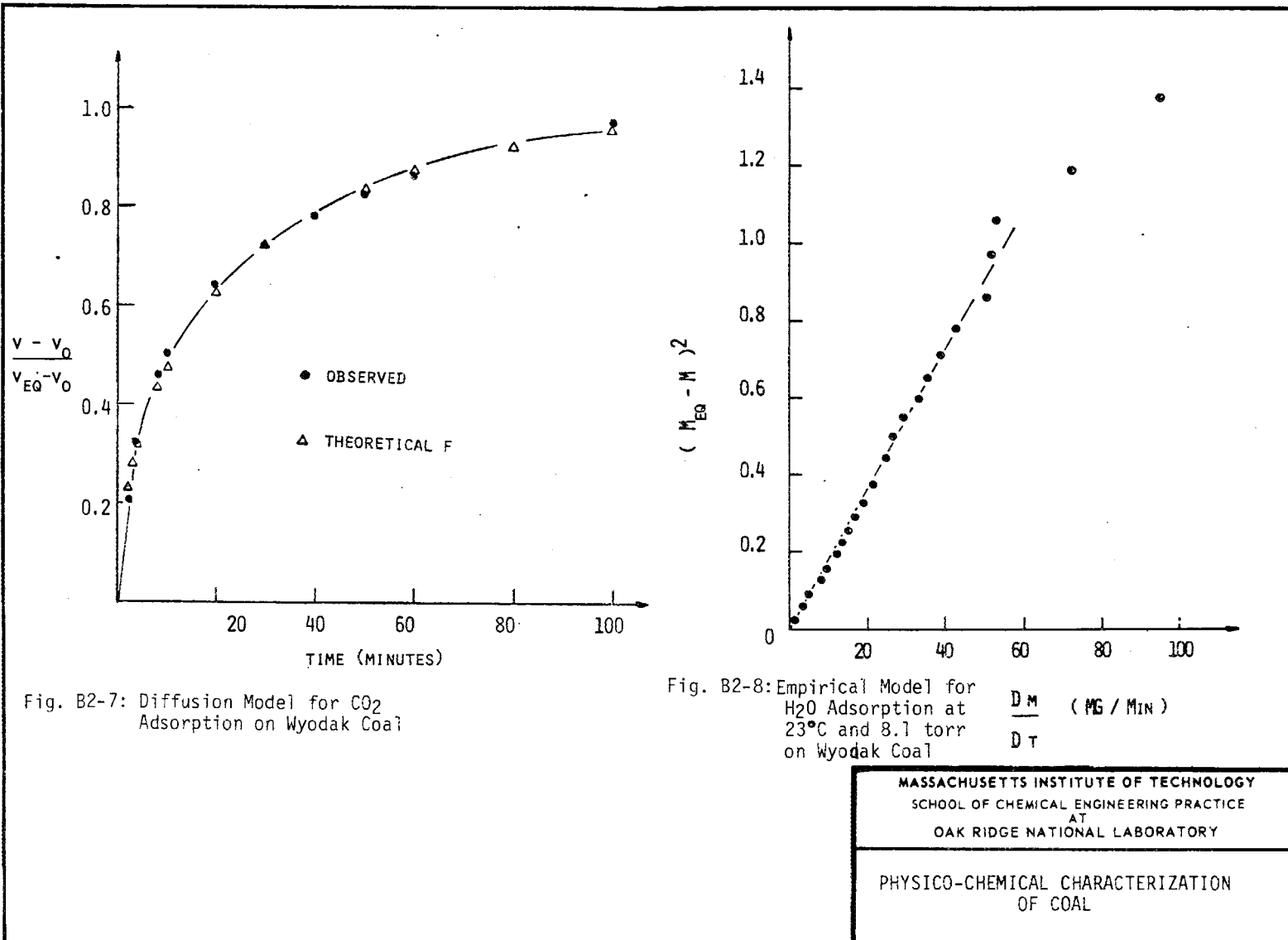


Fig. B2-6: H₂O Sorption Isotherms, I-6 Coal

MASSACHUSETTS INSTITUTE OF TECHNOLOGY
 SCHOOL OF CHEMICAL ENGINEERING PRACTICE
 AT
 OAK RIDGE NATIONAL LABORATORY

PHYSICO-CHEMICAL CHARACTERIZATION OF
 COAL



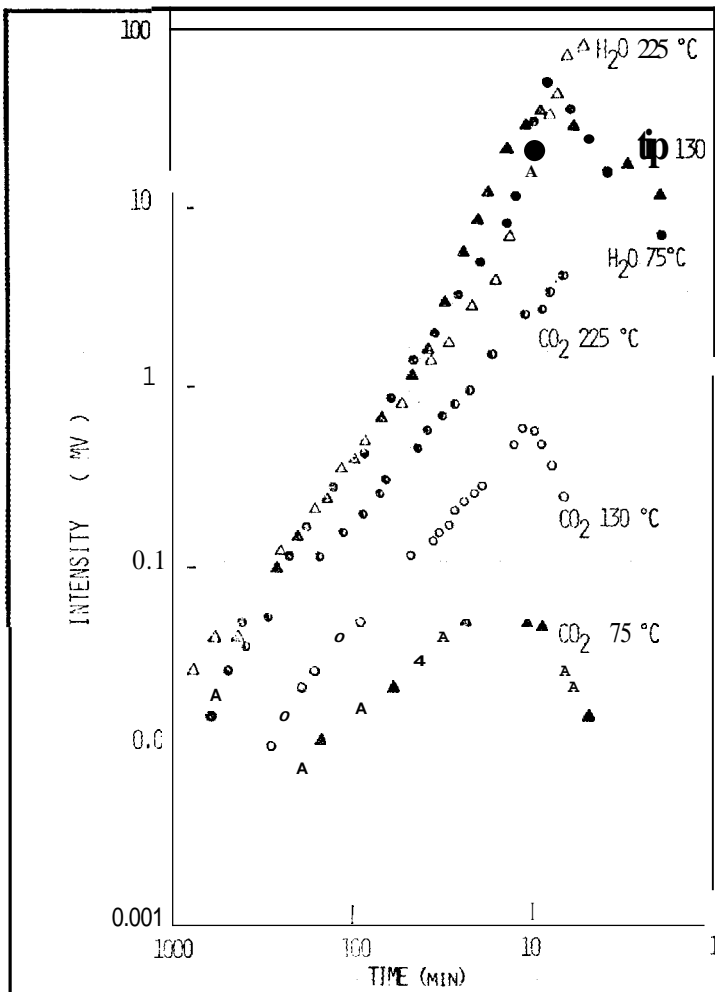


FIG. B2-9: COMPARISON OF INTENSITIES OF EVOLVED SPECIES FOR SEVERAL OUTGASSING TEMPERATURES

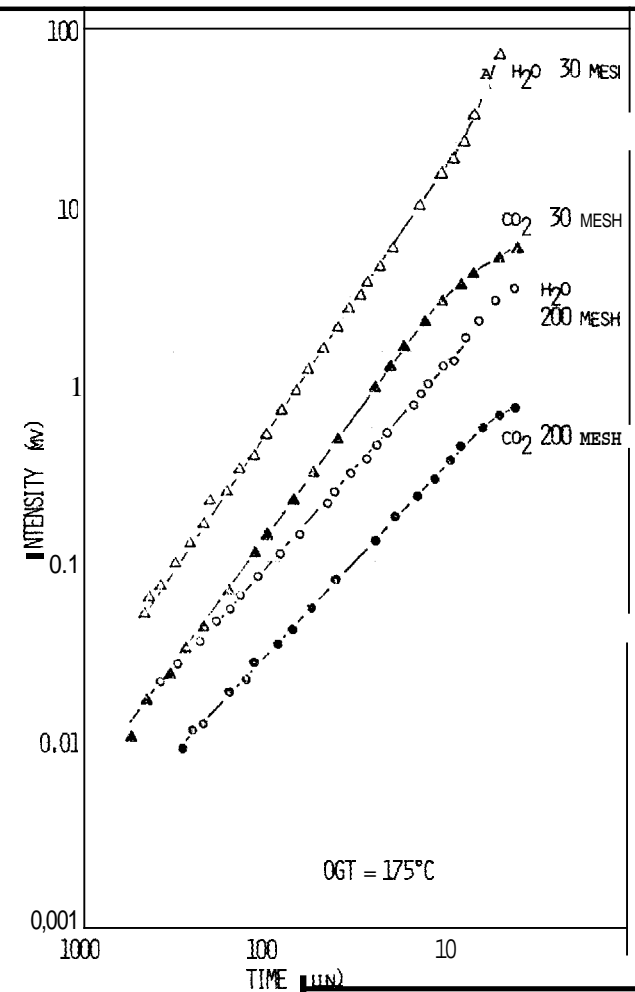


FIG. B2-10: PARTICLE SIZE EFFECT ON OUTGASSING OF WYODAK COAL

MASSACHUSETTS INSTITUTE OF TECHNOLOGY
 SCHOOL OF CHEMICAL ENGINEERING PRACTICE
 OAK RIDGE NATIONAL LABORATORY
 PHYSICO-CHEMICAL CHARACTERISTICS OF COA

$$\frac{dM}{dt} = K(M_{eq} - M)^2$$

where M is the amount of water adsorbed at any time, and M_{eq} is the ultimate H_2O uptake (see Fig. B2-8).

Water is the primary species outgassed (95-99%), and the amount of evolution was independent of temperatures above 25°C. Carbon dioxide was the other major species, with its evolution increasing with outgassing temperature, indicating an activated process (see Fig. B2-9). Total gas evolution decreased for smaller coal particle sizes, suggesting the release of gases during the particle reduction process (see Fig. B2-10).

(1) Hill, G.R., and L.B. Lyon, "A New Chemical Structure of Coal," Ind. Eng. Chem., 54, 36 (1962).

(2) Lowry, H.H., ed., "Chemistry of Coal Utilization," Wiley, New York, 1963.

(3) Marsh, H., and W.F.K. Wynne-Jones, "The Surface Properties of Carbon - The Effect of Activated Diffusion in the Determination of Surface Area," Carbon, 1, 268 (1964).

(4) Van Krevelen, D.W., "Coal," Elsevier, London, 1961.

(5) Alger, M.M., O.K. Chow, and M.Z. Khan, "Surface Properties and Reactions of Coal," ORNL/MIT-266 (Feb. 1978).

(6) Field, L.A., A.J. Papadopoulos, and R.D. Wang, "Surface Properties and Reactions of Coal," ORNL/MIT-270 (March 1978).

(7) Sundberg, D.G., M.J. Abadi, and M.S. Giroux, "Surface Properties of Coal," ORNL/MIT-264 (Dec. 1977).

(8) Caron, R.N., K.J. Fallon, J.F. Ornik, and J.L. Roux-Buisson, "Surface Properties of Coal," ORNL/MIT-273 (May 1978).

3) Dispersion of Miscible Fluids in Porous Media

Dispersion accompanying the flow of miscible fluids through porous media is of fundamental interest in chemical engineering. Effective utilization of enhanced oil recovery methods and chromatographic techniques depend on the proper understanding of this phenomenon.

A displacement is density-favorable and viscosity-favorable when the less dense fluid is above the more dense fluid and when the displacing

fluid is more viscous than the displaced fluid. For density-unfavorable displacements, the mixing zone broadens (increasing the dispersion coefficient) with decreasing fluid velocity; but an increased fluid velocity will broaden the mixing zone of a viscosity-unfavorable displacement. Either viscosity or density effects may be isolated by using fluids which are identical in one of these properties. In some displacements, the conditions of unfavorable density or unfavorable viscosity, packing size, and flow rate may enable "gravity tongues" and/or "viscous fingering" to develop, which greatly increase the mixing zone and dispersion coefficient. They can cause highly irregular concentration profiles across the bed (1).

Experiments were conducted in a vertical column (see Fig. B3-1), packed with spherical glass beads. The density of the effluent was monitored by a densimeter, and the density profiles were matched to model predictions to determine dispersion coefficients for the cases of symmetrical profiles (2, 3). For stable displacements, the concentration of displacing (displaced) liquid in displaced (displacing) one is given by:

$$\frac{\partial C}{\partial t} + v \frac{\partial C}{\partial x} = D \frac{\partial^2 C}{\partial x^2}$$

where D is the axial dispersion coefficient, and x is the axial position. Dispersion coefficients were found to increase with particle diameter, velocity, and density difference (favorable) and correlated well with the difference in Reynolds numbers of the phases as shown in Fig. B3-2.

For unfavorable displacements in which density breakthrough curves were asymmetric, a mixing length was defined as the equivalent column length, in pore volumes, where 90% of the density change occurs, i.e., 5 to 95%. For stable cases the mixing length increases with increasing velocity due to increased micromixing. Conversely, for viscosity-favorable "unstable" cases induced by unfavorable density differences, the mixing length decreases with increasing velocity since increased velocity reduces the time available for gravity tongues to develop. For displacements which could not be classified as "stable" or "unstable," mixing lengths were unaffected by flow rates (see Fig. B3-3). It has been concluded that additional experiments with different pairs of solutions should be made to obtain meaningful correlations for the dispersion coefficients.

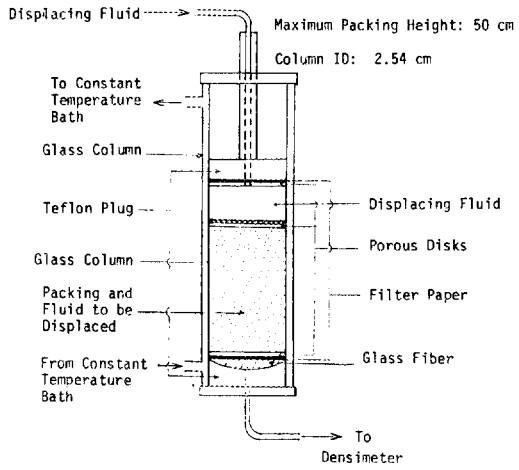


Fig. B3-1: Experimental Column

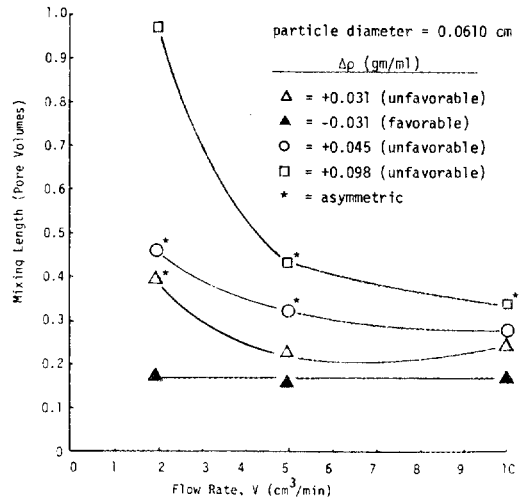


Fig. B3-3: Mixing Length vs Flow Rate

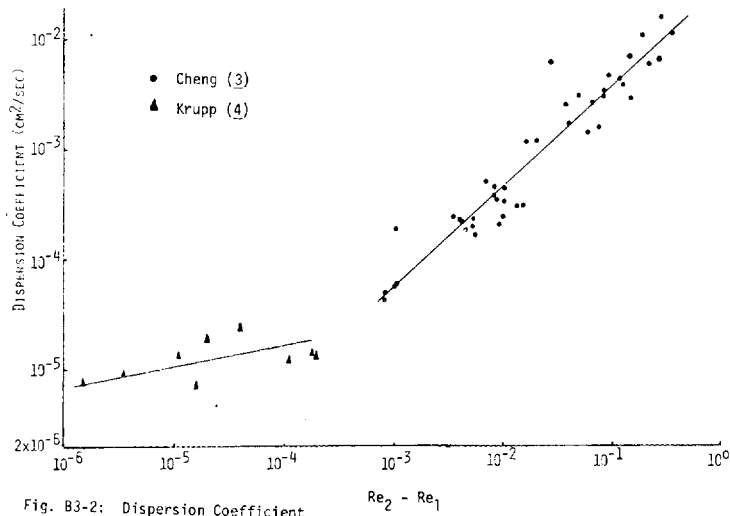


Fig. B3-2: Dispersion Coefficient vs Difference in Reynold Number

MASSACHUSETTS INSTITUTE OF TECHNOLOGY
 SCHOOL OF CHEMICAL ENGINEERING PRACTICE
 AT
 OAK RIDGE NATIONAL LABORATORY
 DISPERSION IN MISCIBLE DISPLACEMENT

(1) Coats, K.H., and B.D. Smith, "Dead-End Pore Volume and Dispersion in Porous Media," Soc. Pet. Eng. J., 4, 73 (1964).

(2) Moor, S.S., S.J. Anderson, B.A. Belt, and J.P. McAleese, "Dispersion of Miscible Fluids in Porous Media," ORNL/MIT-259 (Oct 1977).

(3) Cheng, Y.L., B. Budiman, and M. Machbitz, "Dispersion of Miscible Fluids in Porous Media," ORNL/MIT-276 (May 1978).

(4) Krupp, H.K., "Factors Influencing Miscible Displacement in Porous Media," M.S. Thesis, Dept. of Soil Science, Univ. of Guelph (1966).

4) Recovery of Uranium from Phosphate Rocks

The increase in uranium prices, decrease of easily-recoverable reserves, and predicted increasing demand (1) have stimulated interest in alternative sources of uranium oxide. One likely source is phosphate rock, which contains about 0.38 lb uranium oxide per ton of raw rock. U.S. phosphate rock reserves are estimated to be approximately 7 billion tons, indicating a potentially large reserve of domestic uranium (2, 3).

The economic feasibility of producing uranium oxide from phosphate rock by DEPA-TOPO [di(2-ethylhexyl) phosphoric acid-triethyl phosphine oxide] solvent extraction from wetprocess phosphoric acid (2) was examined using factored estimation methods with an accuracy of $\pm 30\%$ (4). Thirty-eight plants, each producing 1000 tons of P_2O_5 per day (810 lb uranium oxide per day) would produce 5000 tons of uranium oxide per year. Since the first cycle of the DEPA-TOPO uranium extraction process significantly reduces the amount of material handled, the second recovery cycle was centralized to three plant locations, with capital and production costs evenly distributed among the thirty-eight plants. Alternatives examined were (a) the purchase of crude ore or pre-beneficiated phosphate rock, (b) the purchase of sulfuric acid or in-plant production from sulfur or hydrogen sulfide, (c) concentration of the byproduct phosphoric acid to 54% or conversion to diammonium phosphate fertilizer, and (d) recovery of fluorine as fluosilicic acid.

Table B4-1 presents the capital investment required for each sub-process and its alternative. In the recommended case, the purchase of beneficiated rock, production of sulfuric acid from sulfur, concentration of phosphoric acid to 54% and recovery of fluorine result in a total capital investment

Table B4-1. Capital Investment for Process Units and Alternatives

810 lb U ₃ O ₈ /day		<u>\$10³ (1978)</u>
1.	Rock-Beneficiation Facilities	6,090
2.	Phosphoric Acid Plant	15,040
3.	Sulfuric Acid Plant	
	a) From sulfur	18,370
	b) From Hydrogen Sulfide	18,080
4.	Uranium Oxide Extraction* (DEPA-TOPO Process)	5,550
5.	Further Processing	
	a) Phosphoric Evaporator Facilities (to 54%)	257
	b) Diammonium Phosphate Plant	2,840
6.	Fluosilicic Acid Production	820

*Includes complete first cycle and prorated share of centralized second cycle

Table B4-2. Production Cost for Process Units and Alternatives per Pound of U₃O₈

	<u>\$ (1978)</u>	<u>Possible Return \$ (1978)</u>
1.	Beneficiation	109.5
	Or Buy Beneficiated Rock	94.3
2.	Phosphoric Acid	57.7
3.	Sulfuric Acid	
	From Sulfur	77.6
	From Hydrogen Sulfide	140.9
	From Direct Purchase	163.6
4.	DEPA-TOPO Extraction	20.5
5.	Additional Phosphoric Acid Processing	
	To 54%	10.2 395.0
	To Diammonium Phosphate	44.9 200
6.	Fluosilicic Acid Production	2.3 3.2

of 40 million. The inclusion of rock beneficiation facilities would bring the total to \$46 million. The production cost of each processing step and alternative is shown in Table B4-2. The production cost for the optimal case is \$263 per pound of uranium oxide. A profit of \$136 per pound of uranium oxide could be realized if the byproduct phosphoric acid and fluosilicic acid are sold.

It is concluded that the DEPA-TOPO extraction of uranium is economically feasible as an add-on process to existing phosphoric acid plants. Uranium can also be produced profitably as the main product, if the byproducts can be sold or if uranium prices increase sufficiently. As the quality of phosphate rock deposits declines, on-site beneficiation may become less expensive than the purchase of upgraded rock. Similarly, sulfuric acid production from materials other than sulfur, such as hydrogen sulfide, may become more attractive due to growing environmental concerns. Production costs will also increase should the treatment of radioactive wastes in gypsum become required.

(1) "Uranium Industry Breaking Out of the Doldrums," Chem. Eng. News, 11 (May 23, 1977).

(2) Hurst, F.J., W.D. Arnold, and A.D. Ryon, "Progress and Problems of Recovering Uranium from Wet-Process Phosphoric Acid," Paper presented at 26th Annual Meeting, Fertilizer Industry Roundtable, Atlanta, Ga., Oct. 26-28 (1976).

(3) "Superphosphate, Its History, Chemistry, and Manufacture," U.S. Govt. Printing Office (1964).

(4) Wang, R.D., L.A. Field, and F.S. Gillet d'Auriac, "Recovery of Uranium from Phosphate Rocks," ORNL/MIT-26 (Feb. 1978).

C. BIOLOGY DIVISION

Volume Restricted Freezing of Living Cells and Tissues

The ability to preserve living cells and tissues in the frozen state has valuable medical applications in organ and blood banks. Red blood cells, spermatozoa, and other unicellular organisms have been successfully frozen at atmospheric pressure using cryoprotective agents such as glycerol

or dimethyl sulfoxide (DMSO) (1, 2). However, the use of these chemicals can be avoided or minimized by using a constant-volume freezing/thawing process.

The effects of constant-volume freezing on survival of red blood cells and *Artemia Salina* (San Francisco Bay brine shrimp) were examined by immersing samples in stainless steel vessels in constant temperature baths (-40, -78, -196, 37°C) (3). Constant-volume freezing increased red-blood cell survival compared to the constant-pressure process by at least a factor of two, under otherwise similar conditions (see Fig. C-1). The protective mechanism provided by the constant-volume process is, in part, due to reduction in the volume expansion by the formation of ice. Therefore, physical damage to cell membranes is avoided. The use of vessels with larger surface-area-to-volume ratios also improved cell survival rates (see Fig. C-2). The effects of final temperature and cooling/warming rates were determined by conducting two-step experiments. For each vessel geometry, a different cooling/warming history resulted in the highest cell survival rates; however, an initial cooling step in the -78°C bath provided the best results in all cases (see Fig. C-3).

Within the cooling and warming rates investigated, no *Artemia* were successfully frozen and re-animated. However, it was shown that *Artemia* can: (1) withstand pressures greater than 680 atm in the unfrozen state, (2) survive in a 32.5% DMSO solution at room temperature for at least 2.5 hr, and (3) withstand external ice formation (-21°C) for at least half an hour. Additional experiments indicated that a saline solution of 32.5% DMSO undergoes no volume change when frozen.

According to these preliminary results, the constant-volume freezing process should be further investigated. The effects of vessel geometry and cooling and warming rates (temperature and pressure history) on cell survival rates should be quantified.

(1) Farrant, J., C.A. Walker, H. Lee, and L.E. McGann, "Use of Two-Step Cooling Procedures to Examine Factors Influencing-Cell Survival Following Freezing and Thawing," *Cryobiology*, 14, 273 (1977).

(2) Meryman, H.T., R.J. Williams, and M.J. Douglas, "Freezing Injury from 'Solution Effects' and Its Prevention by Natural or Artificial

Fig. C-1: Cell Survival in Constant Volume and Constant-Pressure Freezing

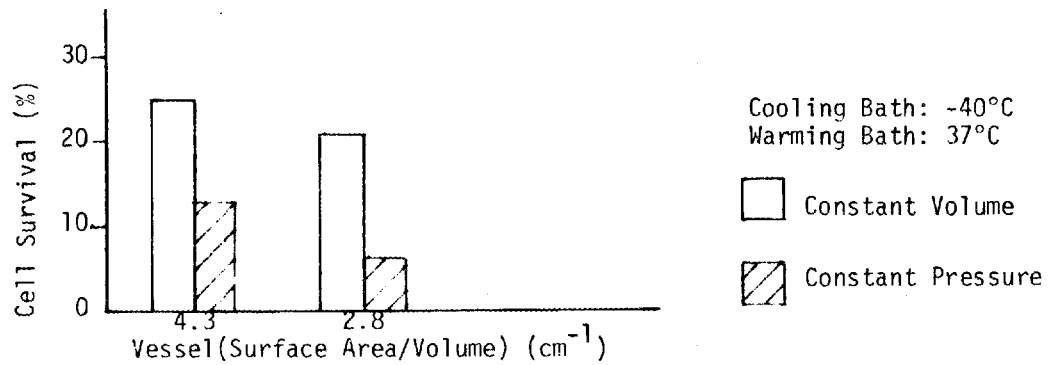


Fig. C-2: Effect of Vessel Geometry on Cell Survival

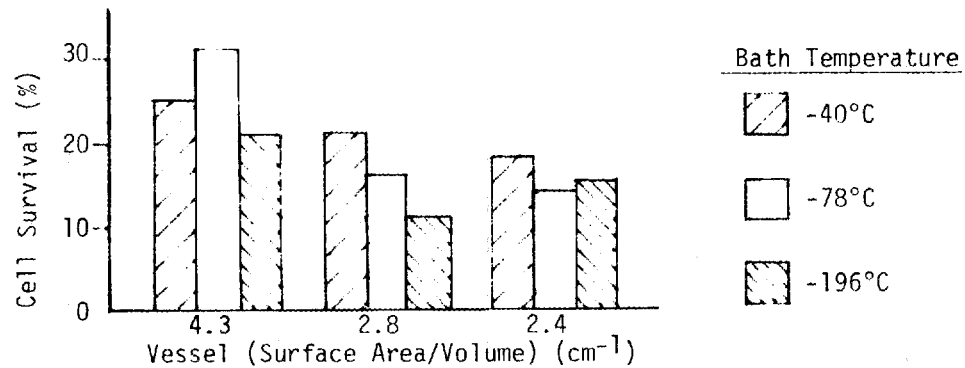
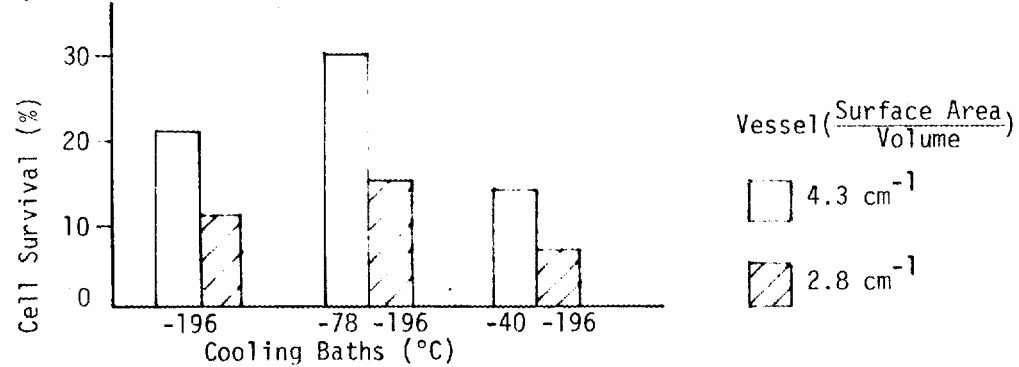


Fig. C-3: Effect of Cooling Rate on Cell Survival



MASSACHUSETTS INSTITUTE OF TECHNOLOGY
SCHOOL OF CHEMICAL ENGINEERING PRACTICE
AT
OAK RIDGE NATIONAL LABORATORY

VOLUME RESTRICTED FREEZING OF
LIVING CELLS AND TISSUES

Cryoprotection," Cryobiology, 14, 287 (1977).

(3) Engstrom, S.D., Y.E. Chu, W.F. Sung, M.S. Giroux, L.W. Bonnell, and G.M. Rinaldi, "Volume-Restricted Freezing of Living Cells and Tissues," ORNL/MIT-265 (Dec. 1977).

D. ENERGY DIVISION

Energy and Cost Analysis of Room Air Conditioners

The growing public interest in energy conservation has encouraged the study of energy efficient technological improvements for household appliances. The ORNL residential energy use model (1) enables policy makers to evaluate energy conservation policies, programs, and technologies for their effects on energy use, energy costs, and capital costs over time. The production-possibilities curve of room air conditioners, relating energy consumption to initial price, is a necessary input to this model.

A baseline unit was chosen (Gibson AL08C4EEBA) that was representative of a large percentage of the units sold in the United States in capacity and EER (Energy Efficiency Ratio, defined as the ratio of a unit's cooling capacity in Btu/hr to the electric power it consumes in W).

Energy savings improvements included the increase of condenser frontal area, the replacement of cooling fins by spines, increases in spine density, increases in the number of coil rows, and decreases in condenser air flow rate. Use of a more efficient four-pole compressor motor and permanent split capacitor fan motor would increase EER by 30% for an additional cost of only 8% as calculated using energy and price models. Further combinations of improvements could increase EER by 53% for a cost increase of 40% (2).

A production-possibilities curve was constructed for the range of technological improvements (see Fig. D-1). The payback period for improving a 6.3 baseline EER unit to a 9.8 EER unit was calculated to be 3.6 yr for New York City and 2.6 yr for Miami based on electricity prices of 7.3 and 3.5 ¢/kWh, respectively.

(1) Hirst, E.A., J. Cope, S. Cohn, W. Lin, and R. Hoskins, "An Improved Engineering-Economic Model of Residential Energy Use," ORNL/CON-8,

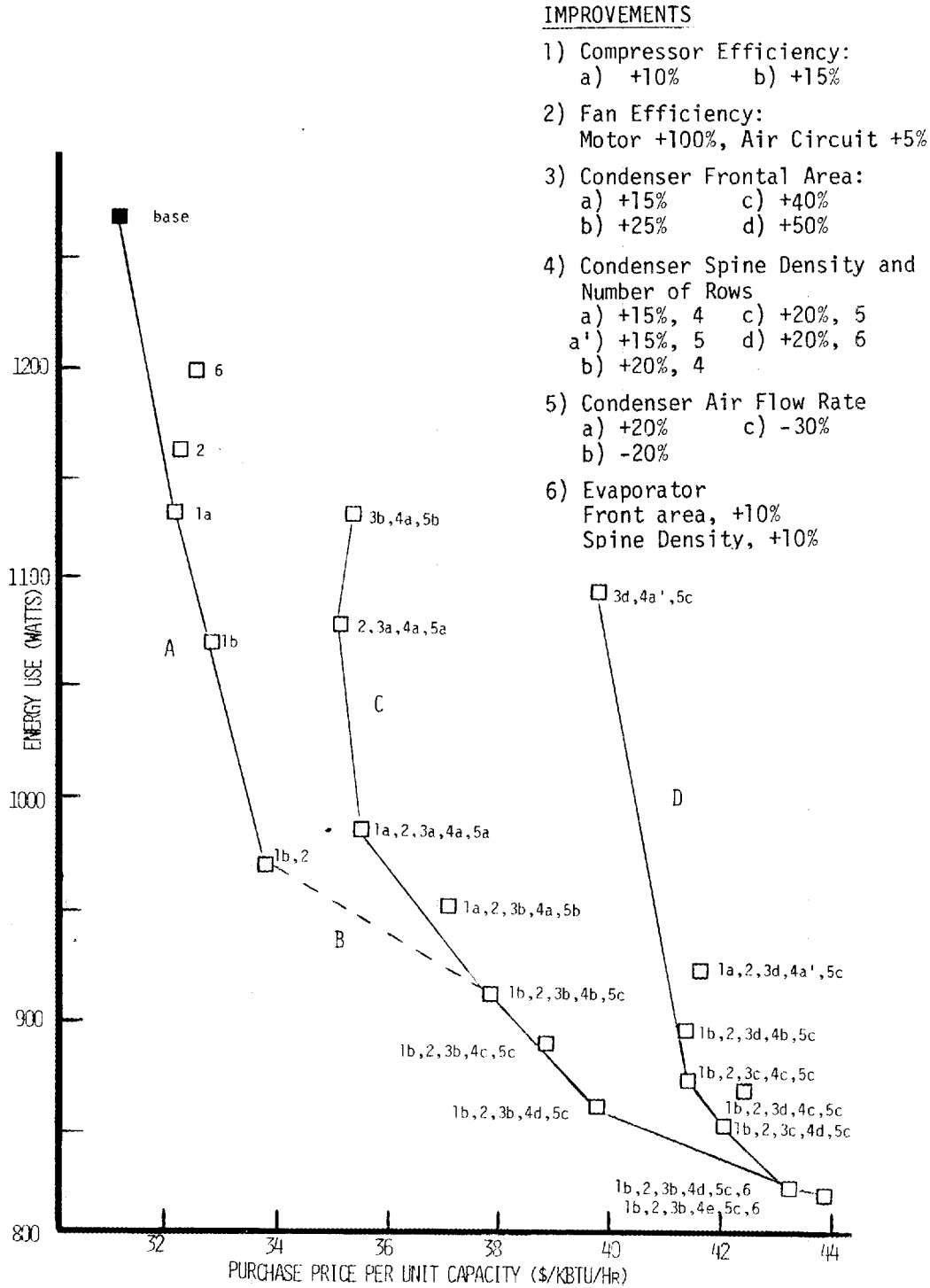


FIG. D-1: PRODUCTION POSSIBILITIES CURVES FOR 8000 BTU/HR ROOM AIR CONDITIONERS

MASSACHUSETTS INSTITUTE OF TECHNOLOGY
 SCHOOL OF CHEMICAL ENGINEERING PRACTICE
 AT
 OAK RIDGE NATIONAL LABORATORY

COST/ENERGY ANALYSIS OF
 ROOM AIR CONDITIONERS

ORNL (April 1977).

(2) Papadopoulos, A.J., and S.A. Berger, "Energy and Cost Analysis of Residential Air Conditioners," ORNL/MIT-268 (Feb. 1978).

E. ENGINEERING TECHNOLOGY DIVISION

1) Radiation Cooling in LMFBR Cores

One possible core-disruptive accident in present design Liquid Metal Fast Breeder Reactors (LMFBRs) is the boiling off of the primary liquid sodium and the subsequent absence of cooling of the reactor core resulting in fuel pin (cladding and then the fuel element) meltdown. When the core is voided, thermal radiation becomes an additional mechanism to cool hot pins by transferring heat to the cold duct wall; this is possible since at moderate temperatures the sodium vapor is practically transparent to radiation (1).

It was assumed that pin failure would occur if the pin surface temperature exceeds the melting point of the cladding of 1644 K (2500°F). The radiosities of the pin surfaces shown in Fig. E1-1 were calculated using the net radiation method (2, 3) along with the other classical considerations. For a particular value of the duct wall temperature, the pin power that maintains the center pin surface at 1644 K was calculated for a range of duct wall temperatures (0 to 1644 K) and for various values of emissivity (0.0 - 1.0), the results of which are also presented in Fig. E1-2.

For a realistic LMFBR accident analysis, heat transfer rates for free and forced convection cooling by sodium vapor were also calculated. These results along with the magnitude of radiation heat transfer are shown in Fig. E1-3. As can be seen, radiation heat transfer (ranging up to 0.33 kW/m) is roughly on the order of free convection (ranging to 0.066 kW/m) and lies below forced convection cooling by the sodium vapor at the designated Reynolds numbers.

The results are strictly applicable for a 19-pin bundle. For the case of uniform radiosity, it has been shown (4, 5) that for the same center pin surface temperature, increasing the number of pins in a given assembly will decrease the maximum pin power allowable. Therefore, the results presented

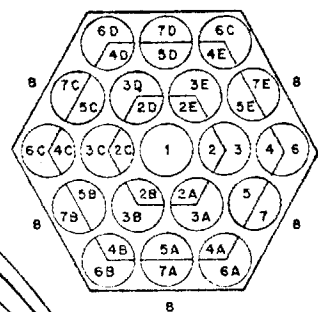
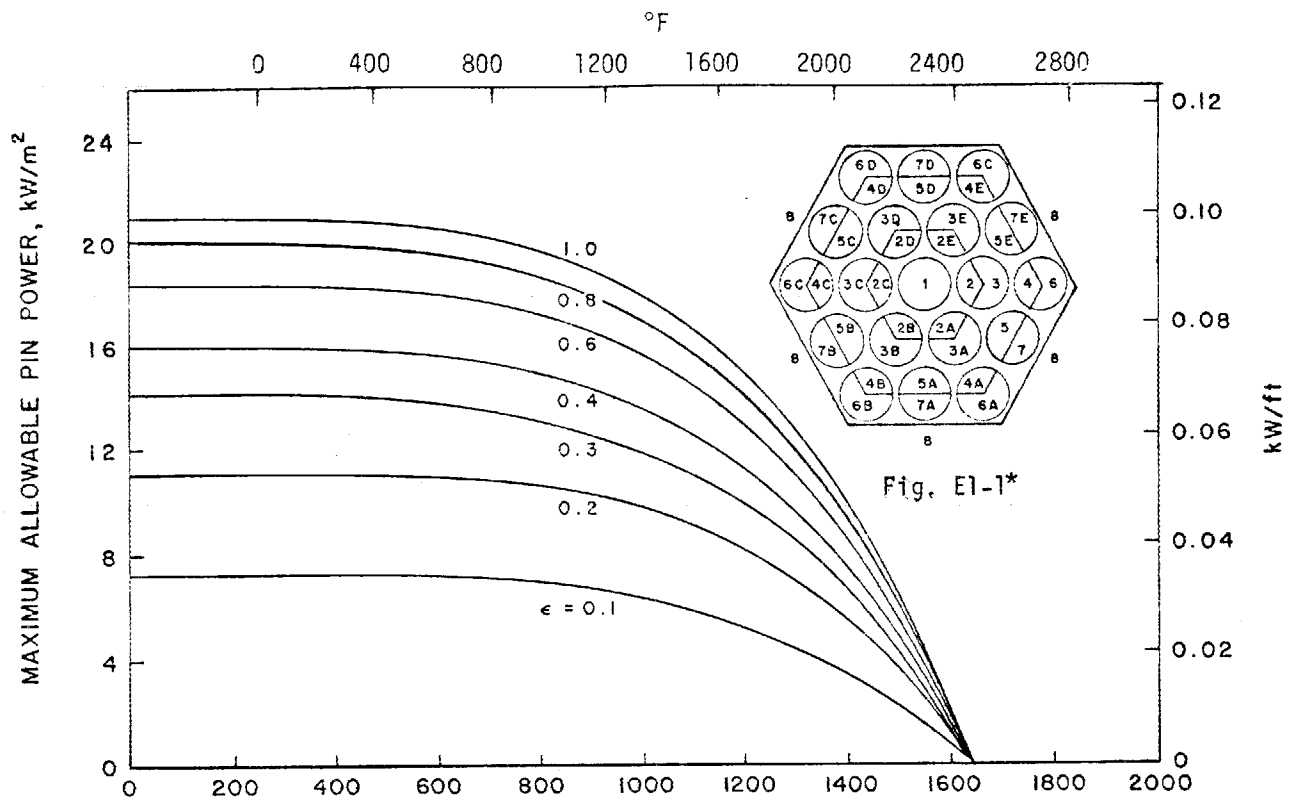


Fig. E1-1*

Fig. E1-2: Maximum Power that Can Be Cooled by Radiation Without Causing Melting

DUCT WALL TEMPERATURE, K

* Fig. E1-1. Cross Section of a 19-Pin Bundle Indicating Radiation Surfaces

MASSACHUSETTS INSTITUTE OF TECHNOLOGY
SCHOOL OF CHEMICAL ENGINEERING PRACTICE
AT
OAK RIDGE NATIONAL LABORATORY

RADIATION COOLING IN LIQUID METAL
FAST BREEDER REACTOR CORES

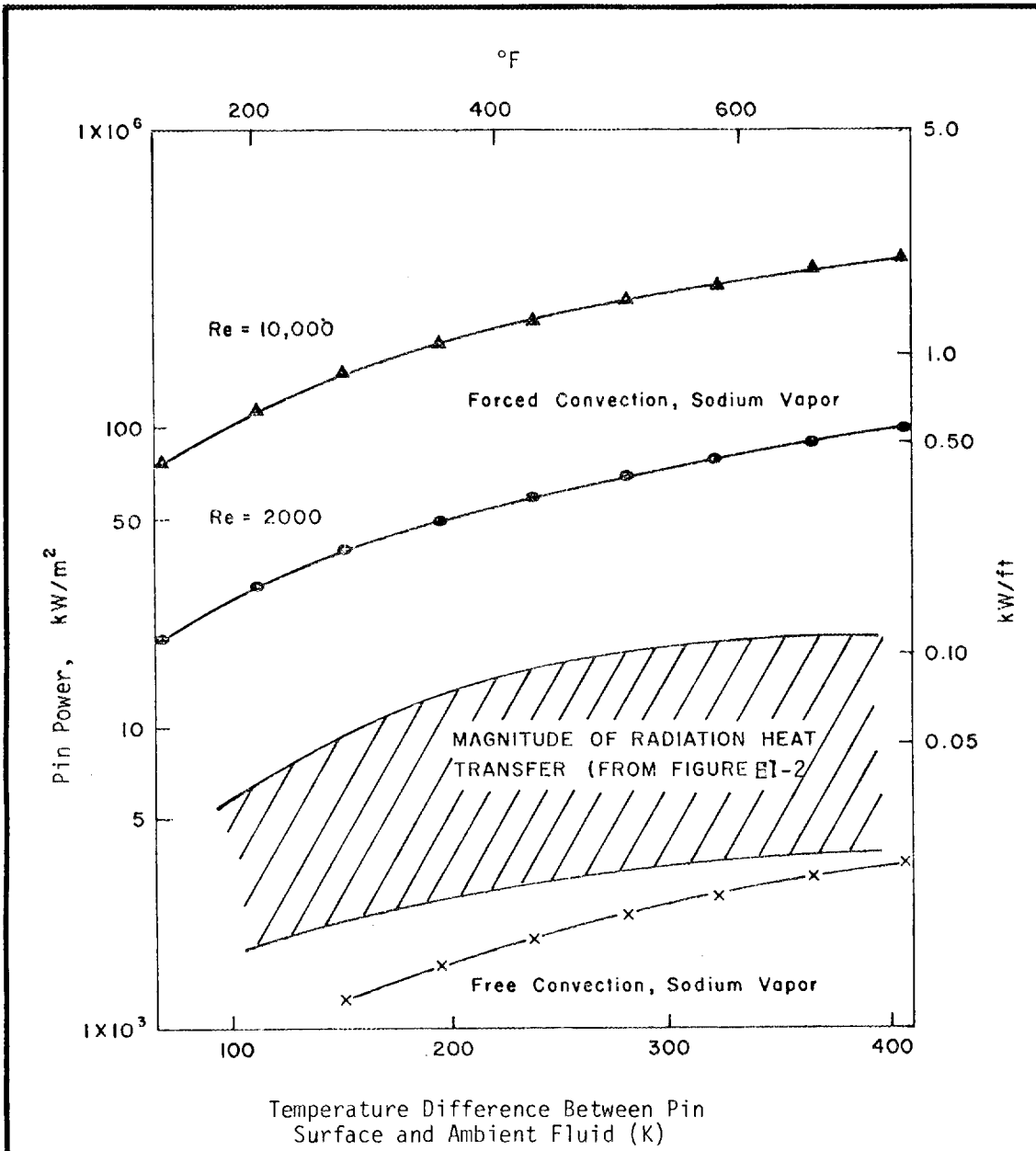


Fig. E1-3: Cooling Capabilities of Various Modes of Heat Transfer

MASSACHUSETTS INSTITUTE OF TECHNOLOGY
 SCHOOL OF CHEMICAL ENGINEERING PRACTICE
 AT
 OAK RIDGE NATIONAL LABORATORY

RADIATION COOLING IN LIQUID METAL
 FAST BREEDER REACTOR CORES

here for the 19-pin bundle are optimistic with respect to the 217-pin fuel assembly in the FFTF and CRBR and place an upper limit on the maximum pin power that can be cooled by radiation heat transfer alone in commercial-scale breeder reactor fuel assemblies. For example, if 32.8 kW/m is the full power load and if the duct wall temperature is 811 K, then from Fig. E1-2 only 0.67% (i.e., 0.22 kW/m) of the total load can be cooled for $\epsilon = 0.4$ by radiation alone.

(1) Machbitz, M., B. Budiman, and Y.Y. Roberts, "Radiative Heat Transfer in a 19-Pin Sodium-Voided Pin Bundle," ORNL/MIT-274 (April 1978).

(2) Cox., R.L., "Radiative Heat Transfer in Arrays of Parallel Cylinders," ORNL-5237 (1977).

(3) Sparrow, E.M., and R.D. Cess, "Radiation Heat Transfer," rev. ed., Brooks/Cole, Belmont, Calif., 1970.

(4) Chan, S.H., *et al.* "Radiative Cooling in a Voided Subassembly," ANL-76-5 (1976).

(5) Chan, S.H., and D.W. Condiff, "Radiative Cooling in a Voided Subassembly," Trans. ANS, 22, 408 (1975).

2) Supercooling of Water in ACES Heat Exchangers

The Annual Cycle Energy System (ACES) supplies space heating and/or cooling using the heat of fusion of ice together with a heat pump (1, 2). To freeze water, systems have been built using heat transfer surfaces submerged in the stored water, as well as systems using external, plate-type ice makers. The former has the disadvantage of requiring large temperature gradients, while the latter process requires extensive refrigeration/heating circuitry to periodically remove the ice from the plates (harvesting). It would be desirable to supercool the water on heat exchanger surface without any ice formation. Existing plate-type ice makers exhibit this supercooling phenomenon for a brief period of time after each harvest. Supercooled water falls onto stored ice below, nucleates, and forms a small pile of slush ice for about 30 sec. Then nucleation occurs on heat exchanger surfaces with the rapid formation of ice.

Nucleation of ice can occur by two different mechanisms: homogeneous (in the bulk) or heterogeneous (on foreign particles or surfaces). Both

involve the creation of ice-water interfaces with the expenditure of free energy, but in heterogeneous nucleation the foreign body allows replacement of ice-water interface with lower-energy, ice-substrate interface, reducing the free-energy barrier to nucleation. Hence, this process becomes the preferred mechanisms,

The free energy of a spherical ice nuclei formation is given by

$$\Delta G = (2 + \cos\theta)(1 - \cos\theta)^2 \left[\pi r^2 \sigma - \frac{\pi}{3} r^3 (\Delta G_v) \right]$$

where σ is the water-ice interfacial tension and θ is the contact angle. The radius corresponding to the maximum value of ΔG is termed the critical radius, r^* . Since minimization of ΔG is thermodynamically favorable, sub-nuclei with radii greater than r^* will grow and initiate bulk crystallization. The amount of supercooling, ΔT , affects ΔG^* by its influence on the free-energy change for phase transformation, ΔG_v . The energy barrier to nucleation, ΔG^* , can be considered as an activation energy (3, 4). The number of nucleation events per unit area of substrate per unit time was shown to be:

$$I \approx 4 \times 10^{23} \exp \left[- \frac{4\pi\sigma^3 T_{mp} (1 - \cos\theta)^2 (2 + \cos\theta)}{3K(\Delta H_v)^2 (\Delta T)^2} \right]$$

This equation shows the large effect of small changes in σ , θ , and ΔT on I . A 0.1°C change in ΔT may increase I by six orders of magnitude. Values of σ and θ cannot be obtained with sufficient precision to make the above equation useful for making predictions. However, it is clear that increasing either σ or θ will contribute to the amount of supercooling attainable before nucleation. Therefore, the rate of nucleation on ice-maker plates depends on (1) the extent of supercooling, ΔT , (2) the water-ice interfacial tension, σ , (3) the contact angle, θ , and (4) pore radius, r .

Attempts were made to reduce the effects of surface irregularities by coating the heat exchanger plates with silicone grease and Teflon film (5). Water flow rate was varied and the extent and duration of supercooling for the coated and uncoated surfaces were measured (see Table E2-1). No improvements in supercooling duration were observed with the coated plate. Additional experiments using a drag-reducing agent in the system water supply

Table E2-1. Supercooling and Duration as a Function of Flow Velocity and Type of Surface Coating

<u>Average Flow Velocity (cm/sec)</u>	<u>Coating</u>	<u>Maximum Supercooling (°C)</u>		<u>Duration of Supercooling (min)</u>	
		<u>Uncoated</u>	<u>Coated</u>	<u>Uncoated</u>	<u>Coated</u>
20	silicone grease	1.2	0.7	n.a.	4.1
20	silicone grease	1.2	0.8	1.0	1.4
20	Teflon film	0.9	none	1.9	0
20	Teflon film	0.3	none	1.3	0
10	silicone grease	2.5	1.0	1.0	1.0
10	silicone grease	2.3	0.8	0.6	1.0
10	Teflon film	0.9	0.4	0.7	1.0

were also unsuccessful in prolonging supercooling.

-
- (1) Fischer, H.C., "The Development of the Ice-Maker Heat Pump," Annual Meeting American Soc. of Heating, Refrigeration, and Air Conditioning Engineers, Seattle, Wash., June 27 - July 1, 1976.
 - (2) Hise, E.C., J.C. Moyers, and H.C. Fischer, "Design Report for the Annual Cycle Energy System Demonstration House," ORNL/CON-1 (October 1976).
 - (3) Kallungal, J.P., and A.J. Barduhn, "Growth Rate of an Ice Crystal in Subcooled Pure Water," A.I.Ch.E. J., 23, 294 (1977).
 - (4) Mason, B.J., "The Supercooling and Nucleation of Water," Adv. Phys., 7, 221 (1958).
 - (5) Rinaldi, G.M., L.W. Bonnell, and C.T. Geary, "Supercooling of Water in ACES Heat Exchangers," ORNL/MIT-263 (Dec. 1977).

F. NUCLEAR MEDICINE TECHNOLOGY

Design of a ^{18}F Production System at ORNL Cyclotron Facility

With the recent developments of positron tomographic imaging devices, the use of radiopharmaceuticals labeled with positron emitting, short-lived radionuclides of ^{11}C carbon, ^{13}N nitrogen, ^{15}O oxygen, and ^{18}F fluorine will make an important contribution to the field of diagnostic and prognostic medical research. The production of these radiopharmaceuticals involves: (a) the selection of a suitable starting material to be used as target material in the accelerator, (b) the nuclear reaction, transforming the target material into the desired radionuclide, and (c) the synthesis of the radiopharmaceutical suitable for clinical use.

A fluorine-18 production system was designed for the ORNL 86-inch cyclotron using H_2^{18}O as the target material (1, 2). Design considerations were target geometry, materials of construction, heat removal, and ^{18}F recovery system. The Accelerator Target Simulation (ATS) computer program was used to determine yields and power dissipation within the target (3, 4). Irradiation time was calculated based on available beam current and level of activity required. The target consists of aluminum and titanium concentric cylinders with target water flowing in the inner cylinder to an external heat exchanger. Target cooling water flows in the annulus removing the

bulk of the dissipated heat. A proton beam current of 250 μA and an irradiation time of 24 min was calculated to be sufficient to produce ^{18}F with an activity of 5 curies without any heat removal problems.

Radiolysis (hydrolysis due to radiation) was calculated to be significant with ~ 0.37 ml/min water decomposing to H_2 and $^{18}\text{O}_2$. Since it is costly to vent these gases, a catalytic recombination unit was designed using a supported palladium catalyst. The catalyst vessel also acts as a reservoir, should target water accidentally be forced from other regions of the system.

A sidestream anion exchange column was designed to recover ^{18}F utilizing the acetate form of highly cross-linked resin which enables 99.9% of the ^{18}F to be recovered within 10 min after the cyclotron run. The total target-water inventory was 240 ml and losses were estimated to be no more than 0.75 ml/run. The complete water-target system, shown in Fig. F-1, will fit on a one-foot-square platform built into the cyclotron dolly, with the heat exchangers fastened to the dolly leg.

In addition, an externally-bombarded $^{18}\text{O}_2$ target was designed to deliver $^{18}\text{F-F}$. An external gas target offers advantages of less target inventory, no radiolysis-related problems, and fewer heat-transfer complications, although the cyclotron must be operated at near full capacity. Suitable conditions to yield one Ci would be a 20- μA beam current with an irradiation time of 47 min.

(1) Shaeffer, M.C., F. Barreto, J.R. Datesh, and B.R. Goldstein, "Design of a ^{18}F Production System at ORNL Cyclotron Facility, Part 1," ORNL/MIT-258 (Oct. 1977).

(2) Chu, Y.J., S.D. Engstrom, and D.G. Sundberg, "Design of a ^{18}F Production System at ORNL Cyclotron Facility, Part 2," ORNL/MIT-262 (Nov. 1977).

(3) Lemon, R.A., B.W. Wieland, R.S. Howell, and J.P. Casillo, "ATS-Accelerator Target Simulation," Oak Ridge Associated Universities (1977).

(4) Lemon, R.A., "ATS User's Manual," Oak Ridge Associated Universities (1977).

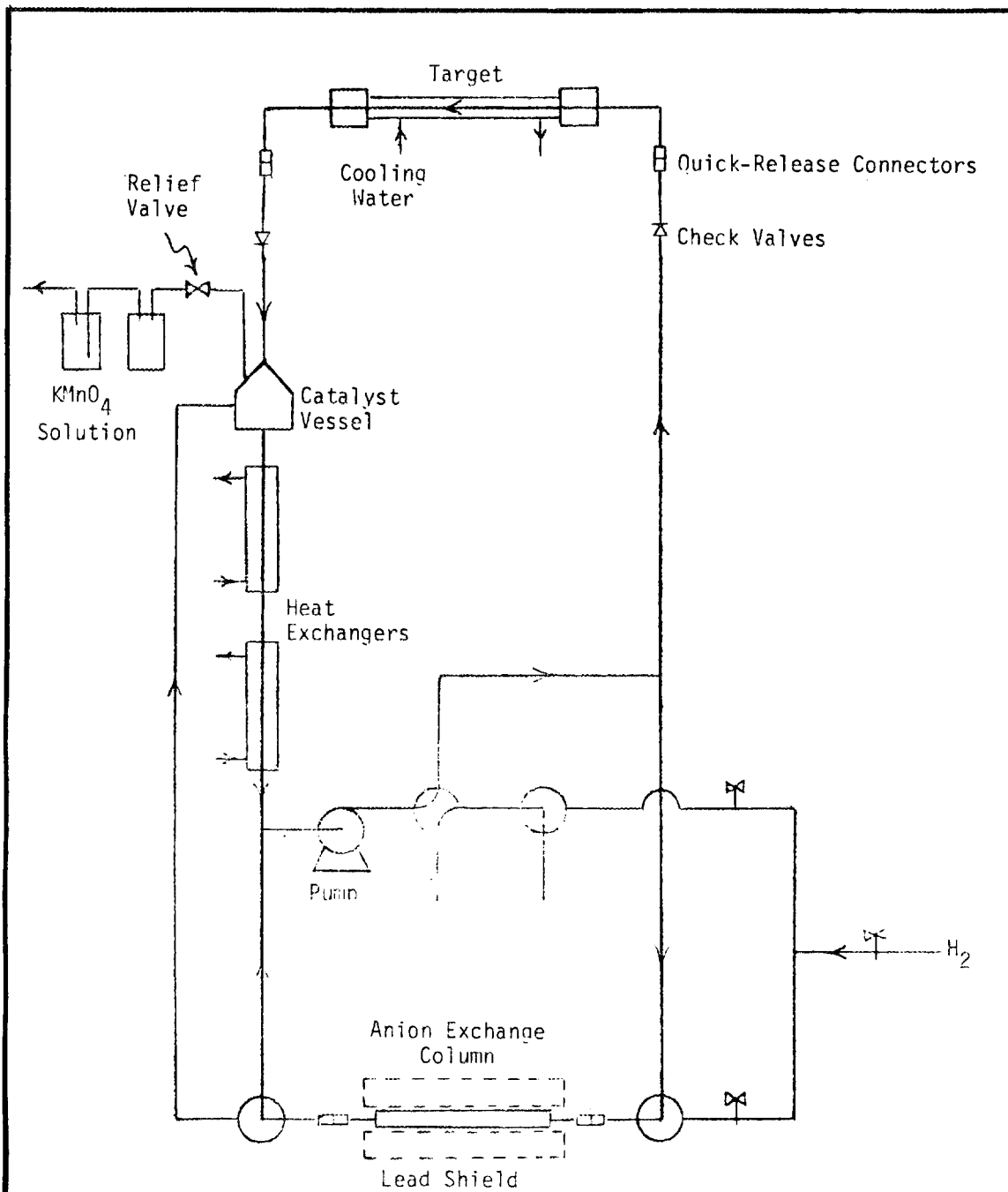


FIG. F-1: WATER TARGET ^{18}F
PRODUCTION SYSTEM

MASSACHUSETTS INSTITUTE OF TECHNOLOGY
SCHOOL OF CHEMICAL ENGINEERING PRACTICE
AT
OAK RIDGE NATIONAL LABORATORY

DESIGN OF A ^{18}F PRODUCTION SYSTEM
FOR ORNL CYCLOTRON FACILITY